J Mater Sci (2016) 51:2199–2242
DOI 10.1007/s10853-015-9537-4

REVIEW

Borate glasses for scientific and industrial applications: a review

Murat Bengisu[1]

Received: 15 June 2015 / Accepted: 26 October 2015 / Published online: 9 November 2015

Abstract Research in borate glasses has started as a scientific curiosity and as an aid to explain the structure of oxide glasses in general. This effort led to a better understanding of the structure and unique properties of borate glasses. Although silicate and borosilicate glasses satisfy the vast majority of scientific and industrial needs, there are certain circumstances where they are not satisfactory. Furthermore, borate glasses offer certain advantages over silicate glasses which are not well known, neither well explored. However, certain characteristics of borate glasses such as their affinity to water requires that they are well selected, designed, or developed to satisfy the specifications of a given application. This review aims to explore and report some of the key properties of binary borate glasses. It also provides certain guidelines for several applications where the scientific literature is discussed in connection with industrial experience and technological needs.

Introduction

The continuous effort for scientific and technological development is a major driving force for the search of materials with improved, tailored, or optimized properties. Although silica glasses satisfy the majority of requirements for a wide range of applications, borate glasses are also getting increased attention because of their unique properties. An important advantage of borate glasses over silica glasses is their significantly lower melting and softening temperatures. Pure B_2O_3 has a glass transition temperature (T_g) of $\sim$260 °C [1] and a melting temperature (T_m) of $\sim$450 °C [2] which are much lower than the corresponding temperatures of $T_g \cong 1100$ °C and $T_m \cong 1728$ °C for SiO_2 [1, 2]. Borate glass is normally not useful for any application in the pure form because of its very low chemical durability and high affinity for water. Therefore, it is used in combination with other oxides such as Al_2O_3 or SiO_2 which leads to improved chemical durability yet at the cost of higher processing temperatures. Nevertheless, certain borate glasses of practical use still have considerably lower melting temperatures compared to silica-based glasses. The low processing temperatures are important in applications like sealing and passivation of electronic instruments [3–5].

The addition of B_2O_3 to SiO_2 glasses led to the development of borosilicate glasses with a broad range of industrial applications. These glasses have higher chemical durability thermal shock resistance, and electrical resistivities compared to soda-lime glasses. The best known example is Pyrex® glass which is used for labware and consumer products such as glass plates and oven ware. The borate content in commercial borosilicate glasses ranges between 13 and 25 wt% [1].

Borate glasses are preferred over silica glasses in sealing applications where the reactivity of silica poses a threat for certain components of the system. For example, silica reacts with sodium in sodium vapor lamps and with lithium available in liquid electrolytes of lithium batteries. Recent studies that aim to develop glass sealants for solid oxide fuel cells (SOFCs) also prefer Si-free glass chemistry since silicon diffusion from silica glass into yttria stabilized zirconia (YSZ) electrolytes has

✉ Murat Bengisu
murat.bengisu@gmail.com

[1] Department of Mechanical and Materials Engineering, Izmir University of Economics, Sakarya Cad. No 156, 35330 Balcova, Izmir, Turkey

the potential to poison the YSZ and reduce its ionic conductivity [6].

It is never sufficient to consider a single parameter for a particular application. For example, sealing applications for electronics require low softening temperatures of the sealing glass in order to minimize damage to electronic components and to reduce production costs. In addition, a glass material used for sealing applications must exhibit a good thermal expansion match and limited chemical reactivity with the base material, strong interfacial bonding, and mechanical strength. Furthermore, certain applications such as SOFC's, aerospace, and biomedicine require hermetic (gas and liquid tight) sealing [7]. The interdependence of certain properties complicates the material selection or product development process. As commonly happens in most design and development activities, the improvement of one parameter could be detrimental to another one. For example, in sealing applications, reducing the melting temperature of the sealing glass may result in reduced chemical durability.

The aim of this review is to bring together available data from the literature, to review some structure–property relationships and to make some extrapolations, interpretations, and recommendations for the optimization and selection of borate glass compositions for selected applications.

Scientific and industrial applications of borate glasses

This section will specifically consider applications of non-silicate glasses based on borates. Critical physical and chemical aspects related to some of these applications will be discussed. Although borosilicate glasses have many important applications, they will not be considered here specifically because the focus of this paper is glass compositions which offer unique properties due to the borate network or borate chemistry.

Sodium vapor lamps, sodium beta batteries, and lithium batteries

Several applications of borate glasses were developed because silica in silicate glasses can be harmed by the chemistry of the application in question. Sodium vapor lamps, sodium-beta batteries, and Li/SO_2 batteries are three such applications. The common denominator of these applications is the alkali element which attacks silica in silicate glasses.

Low-pressure sodium vapor lamps were developed by Phillips and first applied in England to illuminate a road in south London near Phillips Company's research labs [8]. Hot sodium vapor is highly reactive. It attacks and blackens silica-containing glasses. This problem was solved with the development of aluminoborate glasses. However, aluminoborate glasses are attacked by atmospheric moisture, are more expensive, and more difficult to shape. Therefore, only a thin aluminoborate glass coating is currently used inside ordinary soda-lime glass tubing [8, 9]. High-pressure sodium lamps were introduced in the 1970s which employed translucent alumina arc tubes. These lamps had certain advantages over low-pressure lamps such as smaller size and lower cost. Nevertheless, low-pressure sodium lamps are more efficient and they are still being used for street lighting [9].

Sodium beta batteries are rechargeable high-temperature batteries which employ liquid sodium as the active metal in the negative electrode and β''-Al_2O_3 as the electrolyte. One type of sodium beta battery is the sodium/sulfur battery which was introduced in the 1970s. Although this battery was considered for electric-vehicle applications, development programs have ceased in the mid-1990s. However, the sodium/sulfur technology has been utilized by Japanese developers for stationary energy storage applications [10]. In a typical design for a tubular cell battery, a metal case contains the liquid sodium electrode. The β''-Al_2O_3 canister acts as the ion-conducting solid electrolyte which also contains the liquid sulfur electrode [11]. An α-Al_2O_3 ring surrounding the β''-Al_2O_3 tube is bonded by a layer of sealing glass. This glass must resist the corrosive effect of both liquid sodium and sulfur electrodes at the operation temperatures of 290–390 °C.

Another group of sodium beta batteries are sodium/metal halide batteries. Sodium/metal halide technologies were introduced a decade after sodium/sulfur batteries. These technologies offer several advantages over sodium/sulfur battery technologies. Instead of molten sulfur, a metal halide such as nickel chloride or iron chloride is used in the solid state.

Requirements for the sealing glass in sodium beta batteries include [12]

- corrosion resistance against liquid sodium and metal halides,
- hermetic sealing,
- thermal expansion match with α- and β''-Al_2O_3, and
- high bond strength of glass to ceramic joints.

During the initial stages of development, it was realized that silica glasses are unstable against liquid sodium. This problem was addressed by extensive research programs to develop alternative sealing glasses [11]. Most of the work by different groups led to the development of aluminoborate glasses for these applications. Although the amount of glass material used in battery applications is relatively small, sealing glasses are one of the key enablers of high-

performance batteries. Some of the important sealing glasses used in battery and other applications are summarized in Table 1.

There are various types of lithium batteries produced for the consumer market and for industrial applications. The most common type used in the consumer market uses lithium metal as the anode and manganese dioxide as the cathode. This type of lithium battery does not require a glass to metal hermetic seal because it does not involve any pressure of reactant materials. Some types of lithium batteries involve soluble cathodes such as sulfur dioxide (SO_2) or thionyl chloride ($SOCl_2$) and nonaqueous liquid electrolytes such as lithium bromide/acetonitrile (in the case of an SO_2 cathode) and lithium tetrachloroaluminate (in the case of an $SOCl_2$ cathode). The reaction of the cathode and electrolyte materials often causes pressure buildup in the battery cell. Hermetic glass-to-metal seals are commonly used to contain the pressure rise in the cell and to isolate the anode from the cathode [10, 13–15]. Silicate glasses are not a good choice for this application because silica reacts with lithium and forms conductive silicides. Such reactions may both weaken the seal mechanically and cause an electrical short circuit between the battery case (anode) and the pin (cathode). TA-23 glass used for Li ambient temperature batteries contains about 45 wt% silica (Table 1) and resists corrosion for 5–10 years. Alkaline earth aluminoborate glasses have been developed for such applications since they resist attack by alkali metals. CABAL-12 has better corrosion resistance since it does not contain any silica. Glasses used for these applications should have the following properties:

- a good thermal expansion match to the metal components involved,
- good adhesion to the metal components involved,
- corrosion resistance to lithium,
- electrical insulation, and
- a low sealing temperature.

Figure 1 shows a common seal design used in lithium batteries and other similar electrochemical cells. The electrical lead pin is usually made from materials such as molybdenum, tungsten, or tantalum. In addition to being refractory, a common feature of these metals is their low thermal expansion coefficient. CTE values of pure Mo, W, and Ta are listed as 5×10^{-6}/°C, 5×10^{-6}/°C, and 7×10^{-6}/°C, respectively [16]. This level of thermal expansion is easier to match by commercial sealing glasses like TA-23 and CABAL-12, which have CTE values in the order of 6×10^{-6}/°C (Table 1). However, alternative borate glasses with higher CTE values have also been developed to match the higher thermal expansion of certain pin materials such as 446 stainless steel and Alloy-52 with CTE values of 11.4×10^{-6}/°C and 9.8×10^{-6}/°C, respectively. These are boroaluminate glasses with SrO and BaO substituted for the CaO and MgO used in CABAL-12 [17].

Sealing of the viscous glass to the metal occurs at high temperatures leading to the formation of an oxide layer on metal components. Usually this oxide layer is an essential part of a hermetic seal. Glasses with B_2O_3 content above 15 % are known to produce strong adhesion to metals due to the low surface tension of B_2O_3 and a suitable oxide layer formed on the metal. The persistence of adhesion also depends on the thermal expansion match. Even if there is no ideal match between the CTEs of the glass and metal, various design strategies can eliminate the possibility of stress buildup or destruction of the interface bond [18].

The seal must be an electrical insulator to prevent electric flow between the terminal pin and the header body. This requirement is readily satisfied by borate sealing glasses.

Solder glasses

Another major field of application is low temperature sealing glasses also called *solder glasses* or *frit glasses*. These glasses have a softening point below 550 °C. They are employed for sealing, packaging, passivation, and enameling. Industrial sectors which require solder glasses are mainly electronics, electrooptics, mechatronics, and electrical industries. Frit glass is used in the form of glass powder with some polymeric binder and can be applied as a paste. It is also an important material for jewelry, decoration, and ceramics industries. In electronics packaging industries, solder glasses are used for sealing vacuum fluorescent displays, lamp bulbs, plasma display panels, aluminum IC packages, and ferrites. They are also used as insulation coating and overcoating, and for fixing optical communication devices. Almost all commercial solder glasses used to contain lead until recently (Table 1) but the industry is being forced to move away from the use of lead due to its toxicity [19]. Some lead-free glasses with low T_g and sufficient chemical durability include Zn–borophosphate, Zn–Sn–borophosphate [15], SnO–ZnO–P_2O_5 [20, 21], and alkali aluminophosphate glasses [15]. Borate glasses may be preferred in solder glasses for various reasons. Advantages include low melting and application temperature, low viscosity at working temperatures, and low toxicity [22].

Optical and optoelectronic applications

Non-silicate glasses are preferred over silicate glasses in certain optical, optoelectronic, and photonic devices due to their unique properties. Mass production of specially formulated glasses based on borate, phosphate, vanadate,

Table 1 Commercial glass types used for sealing applications

Manufacturer	Commercial designation	Type of glass	Composition (wt%)										
			PbO	B_2O_3	ZnO	Al_2O_3	SiO_2	Na_2O	MgO	CaO	SrO	La_2O_3	CoO
Sandia National Laboratories	Cabal-12	CaO-aluminoborate		41.24		30.20			11.94	16.62			
Sandia National Labs	TA-23	Borosilicate		8.0		20.0	44.95		7.0	12.0	6.0	2.0	0.05
GE	GE 2093	Aluminoborosilicate											
GE	GE 2112	Aluminoborosilicate											
Corning	7570	Lead aluminoborate	75.3	9.5		11.4	3.8						
Corning	8463	Lead borate											
Philips	Solder glass	Lead borate	80	16	4								
Schott	8465	Lead borate											
Schott	8467	Lead borate											
Schott	8468	Lead borate											
Schott	8471	Lead borate											
Schott	8472	Lead borate											
Telefunken	T209	Lead borate	78	14.8		1	5	1.2					
Telefunken	VUS	Lead zinc borate	77.2	12.1	7.8		2.9						
Telefunken	Hard solder glass	Lead borosilicate	30	59	3	1	7						
Telefunken	Hard solder glass	Lead borosilicate	35	50	3		10	P_2O_5:2					
Telefunken	Hard solder glass	Lead borosilicate	38	45	1	1	15						

Manufacturer	Commercial designation	Type of glass	CTE $\alpha \times 10^{-7}$ ($°C^{-1}$)	Deformation temperature (°C)	Sealing temp. (°C)	Materials joined	Applications	References
Sandia National Laboratories	Cabal-12	CaO-aluminoborate	60–68			Mild steel (body or eyelet) to Mo, Ta, or W (pin)	Li/SO_2 and Li/$SOCl_2$ batteries	[14, 115]
Sandia National Labs	TA-23	Borosilicate	63				Electrochemical cells	[18, 116]
GE	GE 2093	Aluminoborosilicate				α-Al_2O_3 to β''-Al_2O_3	Sodium/sulfur batteries	[11]
GE	GE 2112	Aluminoborosilicate				α-Al_2O_3 to β''-Al_2O_3	Sodium/sulfur batteries	[12]
Corning	7570	Lead aluminoborate	84	440	560	Silicon to silicon	MEMS packaging	[18, 117]
Corning	8463	Lead borate	104	377			Ferrite sealing	[118]
Philips	Solder glass	Lead borate	96	420			Sealing and joining of electronic, electrical, and optical components	[119]
Schott	8465	Lead borate	82	T_g: 385	520		Same as above	[118]
Schott	8467	Lead borate	91	T_g: 354	490		Same as above	[118]
Schott	8468	Lead borate	96	T_g: 340	450		Same as above	[118]
Schott	8471	Lead borate	106	T_g: 332	440		Same as above	[118]

Table 1 continued

Manufacturer	Commercial designation	Type of glass	CTE $\alpha \times 10^{-7}$ ($°C^{-1}$)	Deformation temperature (°C)	Sealing temp. (°C)	Materials joined	Applications	References
Schott	8472	Lead borate	120	T_g: 298	410		Same as above	[118]
Telefunken	T209	Lead borate	90	365	410		Same as above	[18]
Telefunken	VUS	Lead zinc borate	91	340			Same as above	[18]
Telefunken	Hard solder glass	Lead borosilicate	50–60		650–700		Same as above	[18]
Telefunken	Hard solder glass	Lead borosilicate	50–60		650–700		Same as above	[18]
Telefunken	Hard solder glass	Lead borosilicate	50–60		650–700		Same as above	[18]

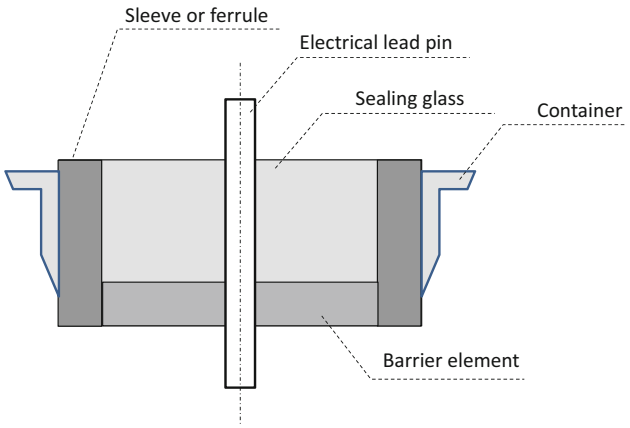

Fig. 1 Cross section of a common seal design used for lithium batteries and other similar electrochemical cells

germanate, or tellurite systems is not feasible but custom made glass components are produced for specific applications and for research purposes in physics, electronics, astronomy, etc. Among such special glasses, borate glasses are of interest mainly for four reasons:

- their low melting temperatures,
- their compatibility with rare earth elements and transition metals,
- their wide glass-forming range, and
- second- and third-order optical nonlinearity.

Borate glasses are capable of vitrifying over a wide range of compositions and host rare earth oxides such as La_2O_3, Pr_6O_{11}, Nd_2O_3, and Sm_2O_3 [23]. One specific application of such glasses is Faraday rotators [24]. The Faraday effect or Faraday rotation is a magneto-optical effect. It involves the rotation of the polarization plane of linearly polarized light under the influence of a magnetic field. The angle of rotation is expressed by

$$\theta = VdH, \tag{1}$$

where θ is the angle of rotation (rad), V is the Verdet constant (rad/T-m), d is the length of the light path through the magnetic field (m), and H is the magnetic field strength (T). Depending on the ions incorporated in them, glasses typically exhibit either diamagnetic or paramagnetic behavior. Diamagnetic glasses commonly have a small positive Verdet constant with a small dependence on temperature. On the other hand, paramagnetic glasses have large, negative Verdet constants which are generally inversely proportional to temperature. According to the specific need in a device, diamagnetic or paramagnetic glasses may be preferred. However, paramagnetic glasses that contain a high concentration of rare earth ions exhibit large Verdet constants and large regions of transparency in the spectral range involved, which broadens the range of applications. Most optical silica glasses are diamagnetic

and exhibit Verdet constants between 4 and 30 rad/(T-m) measured at 633 nm [25]. Although some special silica and other diamagnetic glasses have relatively high Verdet constants, they may cause self-focusing of an intense laser beam, which is not suitable for a high power laser system [26]. On the other hand, rare earth ion containing glasses with low refractive indices may solve this problem. Furthermore, the Faraday effect can be increased by lowering the temperature of the medium, which would increase the possibilities. Verdet constants of −71 and −30 rad/(T-m) have been reported at room temperature for Tb^{3+}-doped (Hoya FR-5) and Ce^{3+}-doped (Hoya FR-4) borate glasses, respectively [27]. A comparison of Tb^{3+}-doped borate, fluoride, and fluorophosphate glasses indicated that the borate glass exhibited the largest Verdet constant [26].

Nonlinear optics is a growing field of science and technology where special glasses and other transparent materials are needed. Applications of nonlinear optical phenomena include frequency generation, optical communication, optical switching, and optical computing [28].

In linear optics, the refractive index of a medium remains constant and polarization of light obeys a linear dependence to an external optical electric field E [27],

$$P = \varepsilon_0 \chi^{(1)} E, \tag{2}$$

where ε_0 is the permittivity of vacuum and $\chi^{(1)}$ is the linear susceptibility, expressed by,

$$\chi^{(1)} = n^2 - 1, \tag{3}$$

where n is the refractive index of the medium in which light travels. Glasses which exhibit linear susceptibility have passive uses such as optical fibers. However, some glasses have been shown to exhibit optical nonlinearity at very high light intensities typically involved with high intensity lasers. This effect is mostly observed in glasses containing highly polarizable ions and exhibiting high refractive index [25]. Non-linear polarization is expressed by a power series [27];

$$P = \varepsilon_0 \left(\chi^{(1)} E + \chi^{(2)} E^2 + \chi^{(3)} E^3 + \ldots \right), \tag{4}$$

where $\chi^{(2)}$ and $\chi^{(3)}$ signify second- and third-order susceptibility, respectively. Second- and third-order nonlinearity in glasses have potential applications such as planar waveguides, active optical fibers, photonic modulators, optical data storage, telecommunication, spectral extension of laser sources, and optical switches [27, 29, 30].

The refractive index of materials that exhibit third-order susceptibility is described by,

$$n = n_0 + n_2 I, \tag{5}$$

where n_0 is the linear refractive index, n_2 is the intensity-dependent refractive index, and I is the laser intensity [31]. The relationship between n_2 and $\chi^{(3)}$ is given by the following equation:

$$n_2 = 5.26 \times 10^{-6} \chi^{(3)} / n_0^2. \tag{6}$$

Here, units of $\chi^{(3)}$ and n_2 are esu and m^2/W, respectively [28].

Even-order optical nonlinearities are forbidden in centrosymmetric materials such as glass. Therefore, second-order nonlinearities are normally not observed in glass. However, in glasses where the macroscopic inversion symmetry is broken, second-order nonlinearity can be observed. The $\chi^{(2)}$ value of thermally and electrically poled fused silica was reported to be as high as 1 pm/V [32]. A recent study showed that second-order nonlinearity in bismuth zinc borate (BZH) glass is limited due to electronic conduction [33]. With the aid of a model which takes into account both electronic and ionic conduction, the $\chi^{(2)}$ value was increased from ~0.5 to ~2 pm/V. Efficient thermal poling could be achieved by using a 3 μm BZH film waveguide on a 150 μm thick glass substrate configuration.

The linear refractive index and third-order nonlinearity in borophosphate as well as La_2O–MgO–B_2O_3 glasses were observed to increase with Ti or Nb concentration. $\chi^{(3)}$ values as high as 55×10^{-22} m^2/V^2 were detected in sodium borophosphate glasses [30]. A comparative study involving praseodymium, neodymium, samarium, and lanthanum borate glasses showed that the best $\chi^{(3)}$ values were obtained in praseodymium borate glasses, ranging from 2.1×10^{-20} to 2.6×10^{-20} m^2/V^2, which are about 60 times larger than that measured for silica glass [23].

Major material selection criteria in nonlinear optics include high nonlinear susceptibility, high transmittance at all wavelengths involved, high resistance to laser damage, high chemical stability, and fast temporal response [31].

Various borate glasses have been studied in order to determine their nonlinear optical properties and to develop suitable glasses for specific applications. Optically stimulated luminescence (OSL) is a method that has been in use since the 1980s and its popularity has been growing ever since. Applications include archeological and geological dating through dose determination in natural materials such as quartz and feldspar, personal radiation dosimetry, and radiation diagnostic imaging [34]. Barium aluminoborate glass was considered as a candidate material for OSL dosimetry because it yields an intense luminescence when stimulated by blue light. A second OSL signal is stimulated by IR, although this is not as intense as the blue light stimulated signal. The OSL signal was reported to show significant fading (30 % in 1000 s) which was considered to be a serious drawback for dosimeter applications. However, there is the possibility of its employment in real time dosimetry [35].

Significant effort has been dedicated to understand the effect of transition metal and rare earth ions on the structure and optical properties of borate glasses. Many glass matrices doped with rare earth ions were demonstrated to operate as efficient luminescent materials and solid state lasers in the visible and near-IR regions. Lead borate and bismuth borate glasses doped with rare earth ions have received considerable attention due to their potential use in laser technology. Pisarska, Pisarski, and coworkers studied the luminescence behavior of rare earth doped lead borate glasses [36–38]. Two characteristic bands were found in the luminescence spectra of Dy-doped lead borate glass; one at 480 nm (blue) due to $^4F_{9/2}$–$^6H_{15/2}$ and the second one at 573 nm (yellow) due to $^4F_{9/2}$–$^6H_{13/2}$ of Dy^{3+} ions. The luminescence bands shifted to longer wavelengths and the yellow to blue luminescence ratios (Y/B) increased with increasing PbO:B_2O_3 mass ratio in $(90-x)B_2O_3$–xPbO-–Al_2O_3–$3WO_3$–$1Dy_2O_3$ (x = 30, 45, 60, 72, 75, and 80 wt%) except for the $18B_2O_3$–72PbO–$6Al_2O_3$–$3WO_3$–$1Dy_2O_3$ system (represented by 1:4). A higher Y/B ratio is usually preferred because the intense yellow emission can be used as a visible solid state laser and raising this ratio also helps to obtain a single line instead of two (blue and yellow) lines [39]. Alternatively, an appropriate combination of these two lines can be used to generate white light by the glass [40]. Increasing the activator (Dy^{3+}) concentration from 0.5 to 3 wt% in the 1:4 system increased the Y/B ratio from 1.05 to 1.15 while reducing the luminescence lifetime from 0.47 to 0.29 ms. Similarly, substitution of PbO by 9 wt% lead halides, PbX_2 (X = F, Cl, Br), in the 1:4 system increased the Y/B ratio from 1.08 to 1.32 while the luminescence lifetime decreased from 0.47 to 0.40 ms [36].

Another Dy^{3+} doped borate system studied in detail with regard to yellow/blue luminescence is the alkali borate glass system $(95-x)B_2O_3$–xNa_2O–5CaO–$0.5Dy_2O_3$. Increasing the Na_2O content from 5 to 30 mol% in this system increased the Y/B ratio from 1.05 to 1.5. Increasing the Na_2O content from 10 to 30 mol% decreased the luminescence lifetime from 0.85 ms to 0.54 ms. A strong correlation was found between the Y/B ratio and Ω_2/Ω_6 ratio, where Ω_t represent Judd–Ofelt parameters [39].

Bi_2O_3 is a heavy metal oxide similar to PbO that has been employed to formulate glass systems with useful nonlinear optical properties. Binary Bi_2O_3–B_2O_3 glass compositions have been studied in detail with regard to their third-order nonlinearity. The large third-order nonlinearity in these glasses was attributed to $[BiO_4]^{5-}$ groups that possess significant hyperpolarization capability.

The effect of TiO_2 addition on nonlinear optical properties in Bi_2O_3–B_2O_3 glass was investigated. It was observed that third-order nonlinearity of such glasses increases with increasing TiO_2 concentration. The highest $\chi^{(3)}$ value obtained was 3.8×10^{-20} m^2/V^2. The main source of nonlinear absorption at 800 nm laser wavelengths was determined to be two-photon absorption [41].

Chen et al. [42] investigated the spectroscopic properties of Bi_2O_3–B_2O_3 glasses doped with Nd^{3+}. The maximum radiative quantum efficiency, stimulated emission cross section, and luminescence lifetime were determined as 54 %, 3.9×10^{-20} cm^2, and 0.095 ms, respectively. Except for the luminescence lifetime, the spectroscopic properties are better than various commercial silicate laser glasses. The same team also studied the spectroscopic properties of Bi_2O_3–B_2O_3 glasses doped with Er^{3+} [43]. In this glass system, the best luminescence lifetime was measured as 0.72 ms while the maximum quantum efficiency and stimulated emission cross section were measured as 25 % and 0.94×10^{-20} cm^2.

Raju et al. [44] studied the optical absorption and NIR emission properties of CdO–Bi_2O_3–B_2O_3 glasses doped with Nb^{3+}. Ω_2 values ranged between 4.893×10^{-20} and 4.248×10^{-20}, which were reported to be significantly larger compared to other glass hosts. Glasses excited by 514.5 nm (Ar^+) laser resulted in NIR emission bands at 900, 1069, and 1338 nm. These bands were attributed to transitions ($^4F_{3/2}$–$^4I_{9/2}$), ($^4F_{3/2}$–$^4I_{11/2}$), and ($^4F_{3/2}$–$^4I_{13/2}$), respectively. The transition at 1069 nm was the one with high intensity. The emission intensity increased as the amount of Nd^{3+} increased from 0.5 to 1.5 mol% but decreased at higher fractions. The stimulated cross section values, calculated as 8.3–15.5 $\times 10^{-20}$ cm^2 for the transition at 1069 nm, were much larger than those reported for commercial laser glasses (ranging between 1.9 and 4.8×10^{-20} cm^2). These studies show that lead and/or bismuth borate glasses doped with rare earth ions such as Dy^{3+} and Nd^{3+} yield candidate glasses for laser applications.

In addition to their role in nonlinear optical properties, it was shown that trivalent transition metal ions (Cr^{3+}) and rare earth ions (Eu^{3+} and Dy^{3+}) can be used as spectroscopic probes for studying the structure and local symmetry of lead borate glasses with different PbO/B_2O_3 ratios [45].

Biomedical applications

The bioactivity of some and the low chemical durability of most borate glasses open up some interesting possibilities in the biomedical field. Bioactive glasses have been used as implant materials for various bone parts and as fillers in dental applications since the 1960s [46]. The prototype material for such applications is known as bioglass or 45S5 which is based on silica as the glass former. Bioactive glasses attach to the bone chemically and form a strong bond. The formation of a hydroxycarbonate apatite (HCA)

or hydroxyapatite (HAp) layer on glass implants or fillers plays a critical role in these applications. Like 45S5 and other silica-based compositions, some borate glasses developed for biomedical applications also exhibit the formation of HCA or HAp at the glass/tissue interface. One example is 13-93B3 glass, which is a Na–K–Ca-borate glass with no silica [47]. The bioactivity of Na_2O–CaO–B_2O_3 glasses with three different compositions was confirmed with XRD; FTIR and SEM analysis. SEM analysis indicated that an interconnected HA network of nearly spherical particles formed on the surface of the glass samples immersed in an aqueous phosphate solution for 3 days. As the molar ratio CaO:B_2O_3 increased, the average size of HA particles decreased, ranging between approximately 6 and 2 μm. However, higher magnification images revealed that these particles actually consist of finer crystals of size 30–70 nm [48].

Although borate glasses were shown to exhibit good compatibility with tissues and support cell proliferation, the high amount of boron ions released during dissolution may become toxic. Nevertheless, it has been reported that small concentrations of boron have an important role in bone formation, maintenance, and regeneration [48, 49]. In order to optimize the dissolution and boron release rate, borosilicate (13-93B1) and strontium borosilicate (2B–6Sr, 2B–12Sr) compositions have been developed. Table 2 shows the composition of various borate glasses considered for biomedical applications. The incorporation of strontium to borate glass was shown to decrease the cytotoxicity significantly [50]. Several in vivo animal studies with bioactive borate glasses reported that no adverse or toxic effects have been observed in the kidney, liver, or blood of the animals [51]. Glasses in the Na_2O–CaO–B_2O_3 system (B18, H12) have been specifically designed for titanium alloys since borate glasses exhibit much better bonding to titanium compared to silica glasses [52, 53]. Some evidence of the cytocompatibility of this family of glass was demonstrated by in vitro cell culture with human mesenchymal stem cells and osteoblasts derived from such cells [54].

Many borate glasses possess biodegradable (or bioresorbable) properties rather than bioactive ones. Namely, they tend to dissolve in aqueous media. Some display both biodegradable and bioactive properties. Biodegradable glasses offer potential use as degradable temporary implants since they dissolve in a controlled manner in the body with the help of the surrounding environment and they are eventually replaced by the desired regenerated tissue [55]. H6b glass exhibited biodegradable behavior in simulated body fluid where the amount of dissolution showed a linear dependence on time [56] while some HAp formation was also observed at the surface. This is a glass based on the Na_2O–CaO–B_2O_3 system, which was developed for biomedical applications [57].

Another potential application of biodegradable glass is controlled drug delivery. Materials presently used for implanted drug delivery systems for the treatment of bone infection or bone regeneration present important disadvantages. Poly(methyl methacrylate) which has been in clinical use for a long time requires additional surgery to remove the inert part after serving as a drug delivery vehicle. Some polymers such as poly(lactic acid) and collagen are biodegradable but they don't form a chemical bond with bone. The degradation of bioactive silica-based glass requires up to 1 year in the body in bone regeneration applications. A calcium borate glass scaffold was developed to serve as a device for drug release in the treatment of bone infection. 90 % of the glass in the device was dissolved within a week and HAp formation was observed. Drug release was completed in 4 days. In vitro and in vivo studies showed that such borate glasses are promising candidates for use as a scaffold and

Table 2 Borate glass compositions developed for biomedical applications

Composition (mol%)	13-93B1[a]	13-93B3[b]	13-93B3/D-Alk-3B[a,b]	2B–6Sr[b]	2B–12Sr[b]	H6B[a]	B18[a]	H12[a]
Na_2O	6.0	6.0	6.0/5.9	6.6	6.7	15.0	12.5	8.0
K_2O	7.9	8.0	8.0/7.9	7.1	6.9	–	–	–
MgO	7.7	8.0	8.0/7.7	1.9	–	–	–	–
CaO	22.3	22.0	22.0/22.2	21.8	17.7	35.0	35.0	40.0
SrO	–	–	–	5.8	11.6	–	–	–
Al_2O_3	–	–	–	–	–	1.0	3.5	2.0
SiO_2	36.3	–	–	19.2	18.8	6.5	6.5	7.5
P_2O_5	1.6	2.0	2.0/1.7	1.8	1.9	1.0	1.0	2.5
B_2O_3	18.2	54.0	54.0/54.6	35.8	36.4	41.5	41.5	40.0
References	[47]	[51]	[47, 58]	[50]	[50]	[57]	[52]	[52]

[a] Measured composition

[b] Nominal composition

local drug delivery device for treating bone infection [58].

Bi et al. [51] studied the effect of bioactive borate glass scaffold morphology and composition on bone regeneration, angiogenesis, and conversion to HA. Glass compositions designated as 13-93B3 (see Table 2) and 13-93B3–Cu (same glass doped with 0.4 wt%CuO) were used. Copper ions are known to promote angiogenesis (formation of blood vessels) and the proliferation of endothelial cells, which are important processes for wound healing. Trabecular scaffolds with a microstructure similar to human trabecular bone have been prepared using a polymer foam replication technique. Oriented scaffolds with columnar pores were prepared by the unidirectional freezing technique. Figure 2 shows the morphologies of trabecular, oriented, and fibrous scaffolds employed. Defects of 4 mm in diameter were created in rat parietal bones. These defects were implanted with bioactive glass scaffolds, which fully converted to HA within 12 weeks. Micro-CT analysis of calvarial defects was conducted after 12 weeks following implantation. Figure 3 shows micro-CT images of bioactive glass implants of different morphologies and compositions. A higher fraction of bone growth was observed in scaffolds with trabecular microstructure. Doping the 13-93B3 glass with copper resulted in a significant increase of new bone growth only in the fibrous scaffolds (15 vs. 33 %, respectively). The amount of blood vessel formation was determined from stained calvarial sections (Fig. 4). The average blood vessel concentration in the cross sections was measured as 4.0 and 4.3 % for 13-93B3 and 13-93B3–Cu trabecular scaffolds, respectively, while it ranged between 2.7 and 3.3 % for other scaffold morphologies. It was also observed that borate glass scaffolds performed better than silicate 45S5 particles used as positive control in this study.

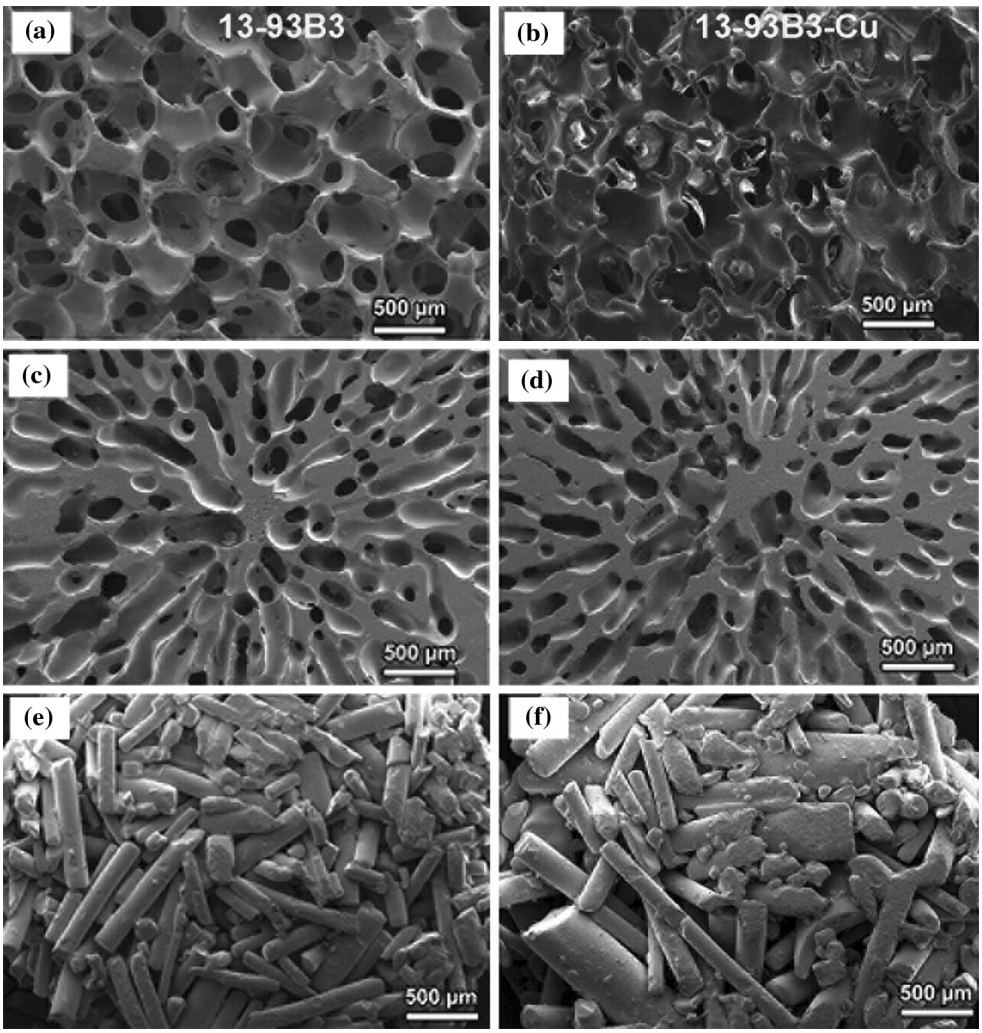

Fig. 2 Morphologies of trabecular (**a**, **b**), oriented (**c**, **d**), and fibrous (**e**, **f**) bioactive glass scaffolds. Reprinted from Ref. [51] with permission from Elsevier

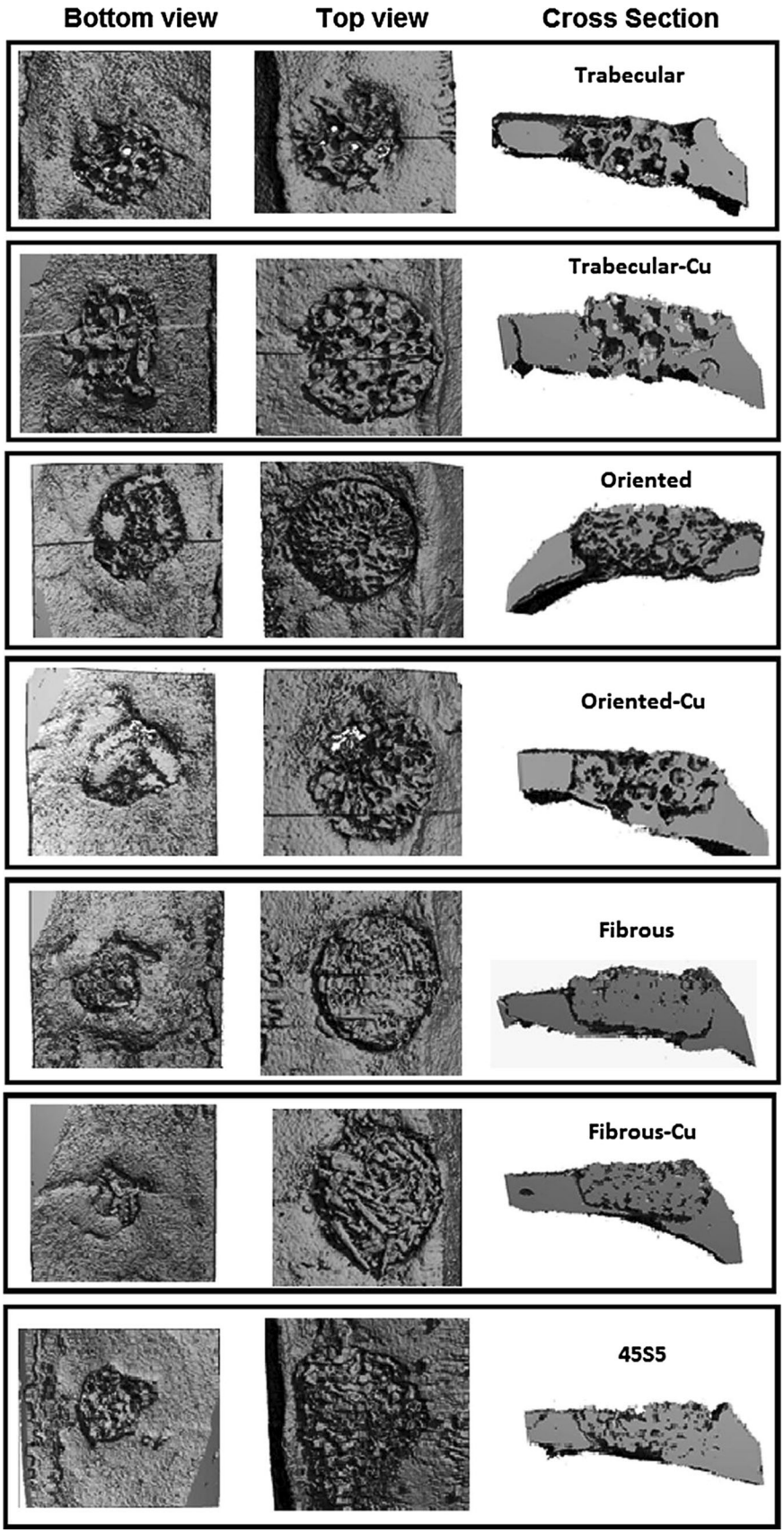

Fig. 3 Micro-CT images of 13-93B3 and 13-93B3–Cu bioactive glass scaffolds with different morphologies and 45S5 particles, 12 weeks after implantation to rat calvarial defects. Reprinted from Ref. [51] with permission from Elsevier

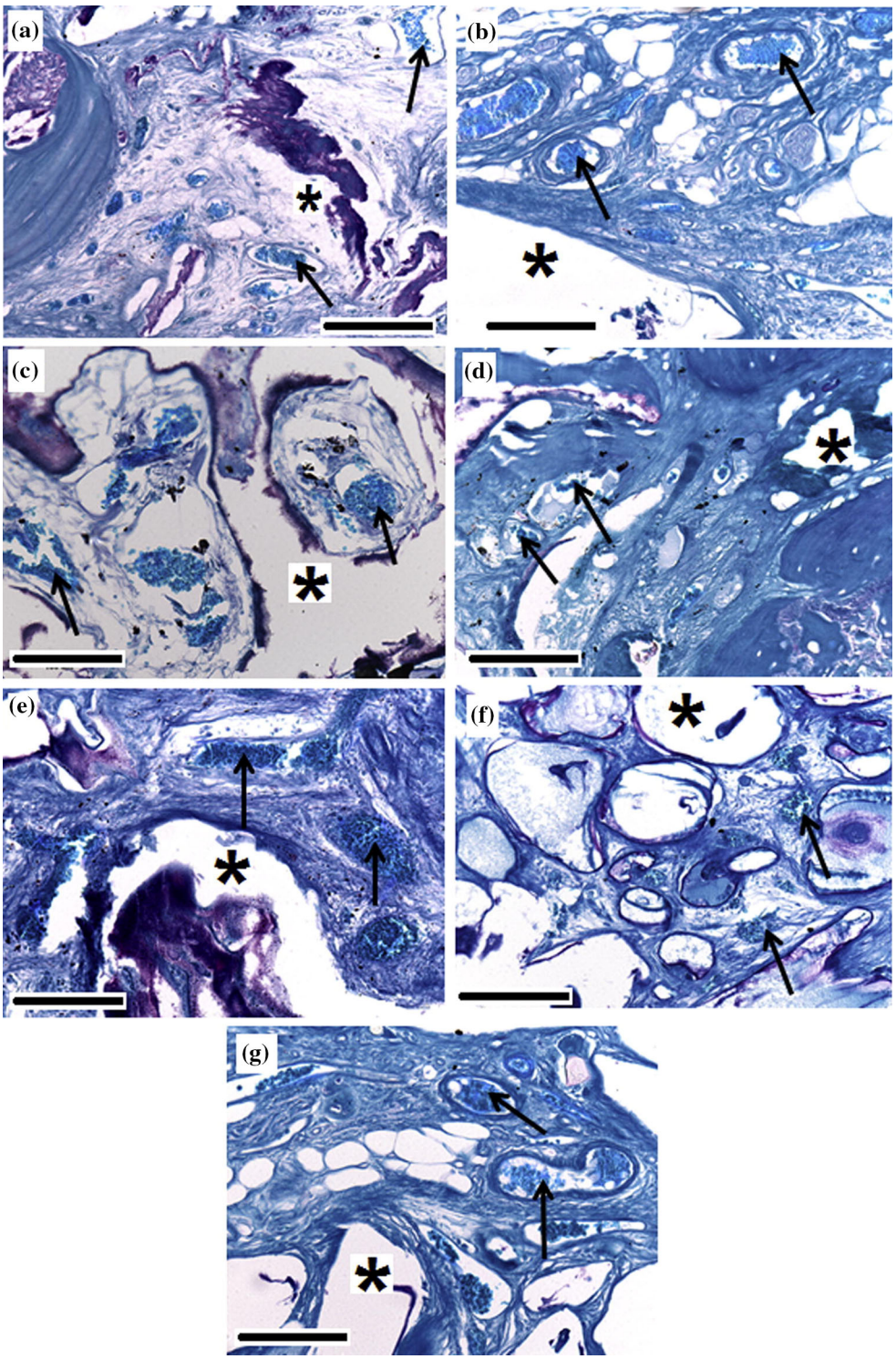

Fig. 4 Micrographs of PAS stained sections of calvarial defects in rats implanted with bioactive glass, 12 weeks after implantation. **a** Trabecular 13-93B3 scaffold; **b** trabecular 13-93B3–Cu scaffold; **c** oriented 13-93B3 scaffold; **d** oriented 13-93B3–Cu scaffold, **e** fibrous 13-93B3 scaffold; **f** fibrous 13-93B3–Cu scaffold; **g** 45S5 particles as positive control. *White areas* marked with (*asterisk*) are remnants of glass scaffolds or particles. *Arrows* indicate blood vessel formation with *red* blood cells colored *green*. *Scale bar* 100 μm. Reprinted from Ref. [51] with permission from Elsevier (Color figure online)

Borate glass delivery systems composed of $6Na_2O$–$8K_2O$–$8MgO$–$22CaO$–$54B_2O_3$–$2P_2O_5$ glass pellets infiltrated with the antibiotic vancomycin were used for the treatment of chronic osteomyelitis in rabbits. The borate glass delivery system was found to be effective for such a treatment [59]. Borate glasses are becoming important in carrier and other biomedical applications because of the important role of boron during embryogenesis and bone growth [60].

Recently a wound healing product was developed by Mo-Sci, a company specialized in precision glass technology. The product with the trade name DermaFuse is composed of borate based glass nanofibers and supplied in the form of bandage-sized pads. It is aimed for treatment of difficult to heal wounds such as venous ulcers experienced by diabetics and pressure ulcers (bedsores) found in bedridden patients or individuals confined to a wheelchair. Initial tests with more than 60 human subjects indicated that the product is successful in healing deep, complicated, and long-standing wounds. The composition of nanofibers are given as 51.5–53 % B_2O_3, 20 % CaO, 6 % Na_2O, 12 % K_2O, 4 % P_2O_5, 5 % MgO, 0–0.4 % CuO, and 0–1 % ZnO (in wt%). Calcium is believed to be an important factor in the healing mechanism, especially in the later stages, because it helps the migration of epidermal cells. The nanofibers create a clot-like structure and provide an antimicrobial environment. Furthermore, it is believed that as the glass is dissolved, various ions, such as Cu^{2+}, are absorbed at the wound site and they stimulate innate cellular and genetic healing processes. [47, 61, 62].

Another borate based glass that is of interest for the biomedical field is antimicrobial glass, developed by the same company. This is a silver containing glass powder with a composition of 40–80 % B_2O_3, 0–70 % P_2O_5, 0–30 %Al_2O_3, 0–12 %Li_2O, Na_2O, K_2O, and 1–30 %Ag_2O (wt%). The antimicrobial effect is provided by silver ions dissolving into aqueous liquids at a rate that is controlled by composition and particle size [62]. One of the biomedical applications of such powders is antimicrobial additives for teeth restoration materials [63].

Calcium sodium borate glass microspheres, 45–90 μm in diameter, produced by flame spheroidization, were transformed into HA as a candidate material for protein separation applications. HA is commonly used in protein separation and purification. The initial spherical shape of glass particles was preserved during transformation. Experiments with bovine serum albumin, chicken egg lysozyme, and horse heart myoglobin indicated that similar protein separation performance could be attained compared to much finer commercial spherical HA particles produced by more complex processes. Spherical particles performed better than irregular particles made of the same material [64].

Radioactive waste immobilization and gamma-ray shielding

A limited number of studies investigated the possibility of using borate glasses as a matrix for high level radioactive waste (HLW) [65–67]. This is a very challenging application since one of the main requirements for such an application is centuries-long integrity and durability of the final product. Although borosilicate glasses are commonly used for nuclear waste immobilization practices, at the absence of silica, borate glasses have very low chemical durability in general, as will be discussed in detail under the section discussing this property. One of the first studies related to nuclear applications of silica-free borates investigated the dissolution rate of CaBAl glass with additions of U_3O_8, Cs_2O, and SrO in water at 70 °C [65] While CaBAl has relatively high chemical durability, the additions of waste oxides reduced the chemical durability significantly. It was suggested that the formation of a Ca-aluminate or $Ca(OH)_2$ gel layer on the glass surface stabilizes the dissolution process. The effect of γ-irradiation on chemical durability was also studied. It was shown that as the dose of γ-irradiation increases, the weight loss increases remarkably during chemical durability tests. Remizov et al. [66] investigated borophosphate glasses as potential materials for HLW immobilization. Boro-organic reagents were used to immobilize liquid HLW in borophosphate glass. However, no detail was given on the dissolution behavior or other properties of the resulting glass.

A recent study reported that lead borate glasses offer some advantages over borosilicate glasses for HLW immobilization applications [67]. Two of these advantages are the low melting points ($T_m < 550$ °C compared to $T_m = 1000$–1600 °C) and lower viscosities compared to borosilicate glasses. It was demonstrated that lead borate glasses with PbO content over 70 mol% demonstrated very limited dissolution. Simulated waste glass samples containing SrO or Cs_2O indicated that an alteration layer seems to inhibit the dissolution of the former while this was not the case in Cs_2O-containing lead borate glasses.

Singh et al. [68] investigated the possibility of using lead borate and bismuth lead borate glasses as a shield for γ-irradiation. The radiation shielding properties of these glasses were shown to be significantly better than various types of concrete at 511 and 662 keV line energies. The mass attenuation coefficient increased almost linearly from about 0.11 to 0.13 cm^2/g as the mole fraction of PbO increased from 0.2 to 0.5 in lead borate glasses. Shielding toward gamma irradiation was also observed in bismuth borate glasses ($60Bi_2O_3$–$40B_2O_3$) especially in the visible region. This was attributed to high density and large atomic number of Bi^{3+} ions and their ability to retard the effects of

gamma-rays [69]. Kaur and Singh [70] studied the gamma-ray shielding properties of lead borate glasses doped with 0.1 mol% Al_2O_3 at a photon energy of 662 keV. Increasing the PbO mole fraction from 0.25 to 0.45 in this system increased the mass attenuation from ~0.092 to ~0.096 cm^2/g. Ruengsri [71] calculated the theoretical gamma-ray shielding properties of borate, silicate, and phosphate glasses containing PbO and compared them to two types of standard shielding concrete. Figure 5 compares the mass attenuation coefficients of three types of glass with varying PbO concentrations and two types of shielding concrete. As seen from this figure, the radiation shielding performance of PbO-containing glasses does not change significantly with respect to the matrix glass. However, all glass materials exhibit better shielding when compared to standard shielding concrete. Thus, PbO and/or Bi_2O_3-containing borate glasses are candidate radiation shielding materials with the advantages of transparency and smaller thickness than concrete shielding components.

Glass-forming ability, glass stability, and crystallization

Obviously the first requirement in applications where glass is a preferable material is the ability to form a glassy (or amorphous) structure in the desired composition. According to the kinetic theory of glass formation, any material can be transformed into glass [1]. The main limitation is the cooling rate from the molten state. The concept of glass-forming ability (GFA) is directly connected to nucleation and crystallization. Shelby defines GFA as "the critical cooling rate required to prevent crystallization of a specified volume fraction of the sample" [1]. This definition is vague because it doesn't tell us what the "specified volume fraction" is. Usually this fraction is related to the technical ability to detect crystals in molten glass and ranges from 1 % to 1 ppm by volume [72, 73]. If a liquid is cooled from the melting (liquidus) temperature, T_m, at a rate higher than the critical cooling rate, R_c, the liquid can form a glass [74]. The slope of the cooling line tangent to the nose of the time–temperature–transformation (TTT) curve (line 2 in Fig. 6) gives the R_c value. A faster cooling rate than R_c will yield a transparent glass (line 1). If the cooling rate is slower than R_c, crystallization will occur (line 3). A system where nucleation and growth of crystals is slower, i.e., where glass formation is easier, yields a smaller R_c value. Thus, the smaller the critical cooling rate of a glass, the better its GFA. Although R_c is a very useful indicator of GFA, it is not readily available for many oxide systems. Calculation of R_c requires experimental TTT diagrams or crystal nucleation and growth rates in a wide temperature region, which are rarely available probably because related measurements are very time consuming [1, 75]. Factors which favor high GFA include a high barrier to nucleation, a high viscosity at the nose temperature of the TTT diagram, and complex melt structures or compositions, since they inhibit the rearrangement of the melt into a crystalline structure [1].

A more useful method, although indirect, is to use thermal analysis data to estimate GFA. The stability of melts against crystallization has been commonly termed glass stability (GS). The same term is also used to describe the resistance of a glass (below the crystallization temperature) against crystallization upon reheating. Nascimento et al. [72] compared critical cooling rates of eight stoichiometric glass-forming oxides with seven different

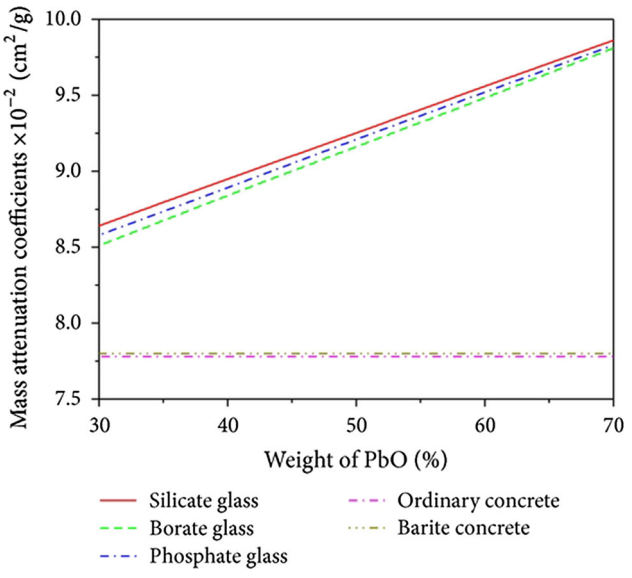

Fig. 5 Increase of mass attenuation coefficient with increasing amounts of PbO in borate, silicate, and phosphateglass at 662 keV photon energy. A comparison is shown with two types of shielding concrete. Reprinted from Ref. [71] (Color figure online)

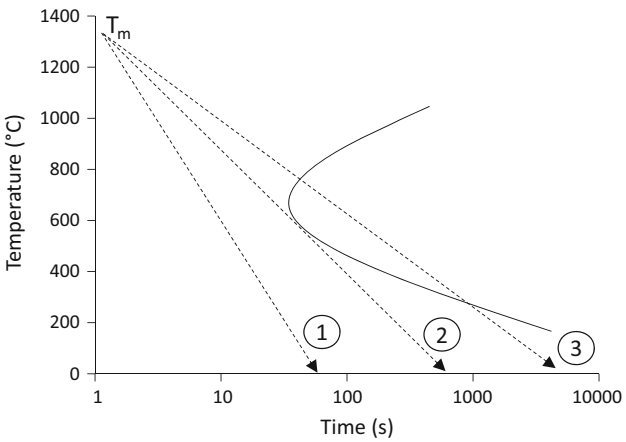

Fig. 6 TTT diagram for a hypothetical glass-forming composition

GS parameters. Six of these glass systems present surface crystallization and two of them bulk crystallization. The study demonstrated that most of the GS parameters that consist of three characteristic DTA/DSC temperatures show excellent correlation with GFA while those which consist of only two characteristic temperatures (T_g and T_m) do not show a good correlation. Comparison of critical cooling rates and GS parameters in these glasses showed an approximately inverse linear relationship between $\ln(R_c)$ and GS parameter K. According to this relationship, as K increases, $\ln(R_c)$ decreases. In other words, as the GS parameter increases, GFA also increases.

Among the six GS parameters tested, three of them, namely the parameters of Weinberg (K_W), Hrubÿ (K_H), and Lu and Liu (K_{LL}) provided the best correlation factors, which were in the range of 0.95 to 0.97. These three parameters are given in Eqs. (7–9), respectively [72].

$$K_W = \frac{T_p - T_g}{T_m} \tag{7}$$

$$K_H = \frac{T_x - T_g}{T_m - T_x} \tag{8}$$

$$K_{LL} = \frac{T_x}{T_g + T_m}, \tag{9}$$

where T_p represents the maximum of the relevant crystallization peak, T_x is the onset temperature for crystallization, and T_g is the glass transition temperature. Using the three parameters given in Eqs. (7–9) and data available in the literature (Table 3), a comparison of GFA and GS in different binary borate glasses has been made (Table 4). Based on these results, it can be inferred that $17Li_2O{\cdot}83B_2O_3$ has the highest GFA and the highest stability against crystallization among the Li_2O–B_2O_3 compositions listed in Table 4. For the PbO–B_2O_3 and Bi_2O_3–B_2O_3 systems, the highest GFA and GS values are expected in glasses with 40 mol% PbO and 25 mol% Bi_2O_3, respectively. The highest GS parameters for three systems listed in Table 4 correspond to the same composition within each system (shown with bold numbers), suggesting a good correlation between different GS parameters. Comparison of the three different systems indicates that, in general, PbO–B_2O_3 glasses have higher GS values, with respect to Li_2O–B_2O_3 and Bi_2O_3–B_2O_3 glasses. This also implies that PbO–B_2O_3 glasses are the easiest to form among these three binary systems.

Phase separation

Even if crystallization can be avoided during or after glass formation, many glass-forming systems are inclined to phase separate [76–78]. Table 5 lists the compositional ranges for glass formation and phase separation for various binary borate systems. Some of the data such as glass formation range and immiscibility range may seem to be conflicting in this table. The reason for this is the different sources used to create it. Glass formation ranges indicate compositions where homogenous clear glass can be obtained. This normally excludes immiscibility ranges where mixed glasses can be obtained by quenching from a region with two immiscible liquids. However, sophisticated techniques are required to be sure whether immiscibility occurs. It has been demonstrated that glasses which appear to be perfectly clear may possess a phase separated structure at the nanometer scale [25]. Phase separation is not necessarily a phenomenon that prevents a glass from being used in an industrial application, but in some cases it may have an unpredictable or undesirable impact on the targeted property. For example, if the phase separated structure has an interconnected morphology instead of isolated spheres in a matrix, and if one of the interconnected phases has a significantly inferior chemical durability, the overall chemical durability will, to a great extent, be determined by the phase with inferior durability. The mechanical properties can also be greatly impaired. In the case of an interconnected morphology, the weaker phase will form the weakest link for fracture and determine the overall strength. If isolated phases are present, a rule of mixture could be used to roughly estimate mechanical properties such as strength, hardness, and elastic modulus [79]. More precise estimations should be based on the Hashin–Shtrikman/Kerner relations since these were shown to best fit phase separated glasses such as sodium silicate and alkali borate glasses [80].

The first thing to consider regarding phase separation in certain borate systems is the phase diagram, if available, and work with compositions which allow glass formation without phase separation. For binary borates, another alternative to consider is to convert a two-phase melt into a single-phase by adding a small amount of a third oxide [18, 81]. Usually, alkali oxides are recommended as the third phase for binary RO–B_2O_3 systems since they act as oxygen donors. For example, more than 3 mol% K_2O is known to eliminate immiscibility in CaO–B_2O_3, SrO–B_2O_3, and BaO–B_2O_3 systems [81].

There are two separate glass formation ranges in some alkali borate systems including Na_2O–B_2O_3, Rb_2O–B_2O_3, and Cs_2O–B_2O_3 (Table 5). The first range (or the only range in the case of Li_2O–B_2O_3 and K_2O–B_2O_3) lies between 0 and roughly 50 mol% alkali oxide while the second range is more limited. In the case of alkaline earth borates, the glass formation ranges are usually narrower. This is partly explained by the high melting points of alkaline earth oxides such as BaO and MgO, which raise the liquidus temperature rapidly with increasing alkaline

Table 3 Some important properties of binary borate systems

Oxide type ** second oxide	mol% second phase	Density ρ (g/cm^3)	Linear thermal expansion coefficient α (10^{-6} K^{-1})	Temperature range (°C)	Molar volume V_m (cm^3/mol)	Glass transition temperature T_g (°C)	Crystallization temperature (onset) T_x (°C)	Crystallization temperature (peak) T_p (°C)
		1.84 [120]						
		1.81 [121]	15 [122]			260 [121]; 258		
Pure B_2O_3		1.804 [123]	8.04 × 10^{-6}/°C [123]	20–300	37.88 [124]	[122]		
Alkali metal oxides								
Li_2O	0.1	1.99 [120]	8.0 [120]					
	0.2	2.15 [120]	6.5 [120]					
		2.23 [120]						
	0.28	2.34 [126]	7.5 [120]					
	1	1.88 [127]			36.84 [127]			
	5.0	1.92 [127]			35.15 [127]	380 [127]		
		1.97 [128]				382 [127]; 355		
	10	1.98 [127]	8.51 [122]	20–300	33.03 [127]	[128]; 336 [122]		
						385 [127]; 397		
	15	2.08 [127]	7.09 [122]	20–300	30.56 [127]	[122]		
	17					457 [129]	575 ± 3 [129]	606 ± 1 [129]
	18					483 [129]	577 ± 1 [129]	610 ± 2 [129]
		2.12 [130]				4165 [131]; 476		
	20	2.11 [128]	7.14 [122]	20–300	29.12 [130]	[128]; 455 [122]	571 ± 0 [131]	587 ± 2 [131]
	21							
	22					506 [129]	569 ± 8 [129]	579 ± 2 [129]
	24	2.17 [130]			27.66 [130]			
						490 [132]; 510		
	25		7.58 [122]	20–300		[129]; 486 [122]	583 ± 7 [129]	589 ± 8 [129]
	27					512 [129]	581 ± 5 [129]	588 ± 4 [129]
	29					513 [129]	573 ± 17 [129]	591 ± 19 [129]
		2.24 [130]				509 [128]; 492		
	30	2.23 [128]	7.89 [122]	20–300	25.81 [130]	[122]; 498 [133]		
	33.3		8.17 [122]	20–300		488 [122]		
	35	2.27 [130]			24.54 [130]			
	37.5							
	40	2.29 [130]	10.04 [122]	20–300	23.48 [130]	468 [122]		690 [135]
	44.4							
	45	2.29 [130]			22.57 [130]			763 [135]

Table 3 continued

Oxide type ** second oxide	mol% second phase	Density ρ (g/cm^3)	Linear thermal expansion coefficient α (10^{-6} K^{-1})	Temperature range (°C)	Molar volume V_m (cm^3/mol)	Glass transition temperature T_g (°C)	Crystallization temperature (onset) T_x (°C)	Crystallization temperature (peak) T_p (°C)
	47.4							
		2.29			21.69 [130]			
	50	[121, 130]			21.72 [121]	417 [121]		
	54.5							
	58.3							
	61.5							
	65							
	70	2.20 [121]			19.00 [121]	312 [121]		
	75	2.10 [136]						
Na_2O	5.4					283 [137]		
	8.7	2.005 [133]				363.6 [133]		
		2.05 [128]				361 [128]; 364		
	10	2.02 [126]	10.01 [122]	20–200		[126]; 344 [122]		
	10.21*	2.047 [138]						
	12	2.069 [133]				409.8 [133]		
	12.4					368 [137]		
	14.28*	2.106 [138]						
	15					409 [137]		
	16	2.141 [133]				457.8 [133]		
	17.4					414 [137]		
	17.5		9.47 [122]	20–300		428 [122]		
	18.3	2.223 [133]				468.2 [133]		
	19							
		2.2264 [185]						
		2.21 [130]			30.584 [138]	487 [139]; 464		
	20	2.18 [128]	9.59 [2]	50–150	30.155 [130]	[128]		
	20.16*	2.186 [138]						
	22.1					475 [126]		
	23.7	2.317 [133]				470.1 [133]		
	24	2.20 [130]			34.38 [130]			
						476 [132]; 468		
	25		10.26 [140]	20–300		[137]; 456 [141]		
	25.7					480 [142]		

Table 3 continued

Oxide type ** second oxide	mol% second phase	Density ρ (g/cm^3)	Linear thermal expansion coefficient α (10^{-6} K^{-1})	Temperature range (°C)	Molar volume V_m (cm^3/mol)	Glass transition temperature T_g (°C)	Crystallization temperature (onset) T_x (°C)	Crystallization temperature (peak) T_p (°C)
	25.99*	2.285 [138]						
	29.1					476 [142]		
	29.91*	2.340 [138]						
		2.3465 [143]						
		2.35 [130]						
	30	2.23 [126]			28.62 [130]	[128]; 470 [137]		
	32.5					468 [137]		
			11.53 [144]; 12.05			462 [144]; 465		
	33.3	2.377 [145]	[122]; 11.53 [133]	20–300	28.20 [145]	[122]		
	33.7					474 [142]		
	33.8		12.69 [2]	20–300				
	35.0	2.41 [130]			27.82 [130]	461 [137]		
	35.8					479 [146]		
	35.94*	2.386 [138]						
	40	2.44 [130]			27.30 [130]			
	40.2					446 [142]		
	50	2.47 [130]			26.61 [130]			
	75	2.39 [136]						
K_2O	1.92				37.01 [124]			
	4.05				36.25 [124]			
	6.14				35.71 [124]			
	8.23				35.33 [124]			
	10.16				35.18 [124]			
	12.27				35.06 [124]			
	14.15				35.01 [124]			
	16.1				34.98 [124]			
	17.8				34.93 [124]			
	19.8		11.75 [2]	20–360	34.85 [124]			
	20	2.14 [130]			34.76 [130]	452 [186]		
	22.06				34.61 [124]			
	25					436 [132]		
	26				34.1 [124]			
	28				33.89 [124]			

Table 3 continued

Oxide type ** second oxide	mol% second phase	Density ρ (g/cm^3)	Linear thermal expansion coefficient α (10^{-6} K^{-1})	Temperature range (°C)	Molar volume V_m (cm^3/mol)	Glass transition temperature T_g (°C)	Crystallization temperature (onset) T_x (°C)	Crystallization temperature (peak) T_p (°C)
	30	2.27 [130]			33.86 [130]			
	33.4		16.03 [2]	15–100				
	34.8					432 [146]		
	35	2.32 [130]			33.72 [130]			
	40	2.32 [130]			34.22 [130]			
	45	2.35 [130]			34.40 [130]			
	50	2.38 [130]			34.49 [130]			
Rb_2O	75	2.32 [136]						
	1.95				37.06 [124]			
	4.05				36.65 [124]			
	9.95				35.91 [124]			
	14.99				36.55 [124]			
	19.97				37.16 [124]			
	22.49				37.05 [124]			
	25				36.87 [124]	423 [132]		
	29.95				36.37 [124]			
	32.46				36.67 [124]			
	37.47				37.43 [124]			
	75	3.50 [136]						
Cs_2O	1.15				37.53 [124]			
	2.18				37.38 [124]			
	4.31				37.14 [124]			
	8.61				37.45 [124]			
	10	2.3 [133]				320 [133]		
	10.83				37.9 [124]			
	14.94							
	18.65							
	20							
	22.72							
	25							
	26.32							
	30.72							
	33							

Table 3 continued

Oxide type ** second oxide	mol% second phase	Density ρ (g/cm^3)	Linear thermal expansion coefficient α (10^{-6} K^{-1})	Temperature range (°C)	Molar volume V_m (cm^3/mol)	Glass transition temperature T_g (°C)	Crystallization temperature (onset) T_x (°C)	Crystallization temperature (peak) T_p (°C)
	34.89							
	75							
Alkaline metal earth oxides								
MgO	16.7							
						280 [121] and		
						642 [121] Phase separation		
	23.1	2.27 [121]						
						286 [121] and		
	28.6					643 [121] phase separation		
	33.3		4.9 [144]	20–300		620 [144]		
	37.5	2.42 [121]				639 [121]		
	44.4	2.44 [121]				632 [121]		
	50.0	2.51 [121]				643 [121]		
	54.5	2.54 [121]				634 [121]		
	58.3					635 [121]		
						279 [121] and		
						631 [121] phase separation		
CaO	9.1							
	16.7					638 [121]		
	20.0							
	23.1					647 [121]		
	25.0		5.93 [140]	20–300		632 [140]		
			7.23 [140]	300–400				
	25.9	2.45 [121]				643 [121]		
	26.3					630 [142]		
	28.6	2.48 [121]				649 [121]		
	29.8					644 [142]		
	30.0		6.30 [140]	20–300		646 [140]		
			7.33 [140]	300–400				
	33.3	2.56 [121]	6.64 [140]	20–300		[140]		
			7.07 [140]	300–400				
	33.5					651 [142]		
	35.0		6.76 [140]	20–300				

Table 3 continued

Oxide type ** second oxide	mol% second phase	Density ρ (g/cm^3)	Linear thermal expansion coefficient α (10^{-6} K^{-1})	Temperature range (°C)	Molar volume V_m (cm^3/mol)	Glass transition temperature T_g (°C)	Crystallization temperature (onset) T_x (°C)	Crystallization temperature (peak) T_p (°C)
			7.84 [140]	300–400		649 [140]		
	40.0		7.29 [140]	20–300		650 [140]		
			8.31 [140]	300–400				
	44.8	2.72 [121]				652 [121]		
						635 [121]; 629		
	50.0	2.79 [121]				[142]		
	55.0	2.80 [121]				613 [121]		
	58.3					595 [121]		
	60.0							
	70.0							
						276 [121] and		
						544 [121] phase separation		
SrO	5.0	2.14 [121]						
						293 [121] and		
						569 [121] phase separation		
	9.1							
	16.7	2.50 [121]				587 [121]		
	28.6	2.92 [121]				637 [121]		
	33.3	3.11 [121]				638 [121]		
	37.5	3.23 [121]				641 [121]		
	44.4	3.42 [121]				628 [121]		
	50.0	3.48 [121]				604 [121]		
	54.5	3.56 [121]				577 [121]		
	61.5					543 [121]		
	64.5					534 [121]		
						284 [121] and		
						491 [121] phase		
BaO	9.1					separation		
	16.7	2.68 [121]				526 [121]		
	23.1					583 [121]		
	25.6					584 [142]		
	28.6	3.35 [121]				603 [121]		
	29.6					593 [142]		

Table 3 continued

Oxide type ** second oxide	mol% second phase	Density ρ (g/cm^3)	Linear thermal expansion coefficient α (10^{-6} K^{-1})	Temperature range (°C)	Molar volume V_m (cm^3/mol)	Glass transition temperature T_g (°C)	Crystallization temperature (onset) T_x (°C)	Crystallization temperature (peak) T_p (°C)
						605 [121]		
	33.3		7.90 [144]	20–300		590 [144]		
	34.4					595 [142]		
	37.5	3.71 [121]				603 [121]		
	39.6					589 [142]		
	44.4	3.95 [121]				576 [121]		
	47.4	4.09 [121]				559 [121]		
	50.4					439 [142]		
	63.0	4.50 [121]				484 [121]	521 [149]	
	64.3					480 [121]	507 [149]	
	65.5					484 [121]	503 [149]	
Transition metal oxides								
ZnO	60.0	3.68 [150]	5.5 [150]		28.5 [150]	440 [150]		
GeO	5	1.902 [123]	15.1 [123]	20-*T*				
	10	1.869 [123]						
	15	2.053 [123]	13.2 [123]	20-T_g				
	20	2.147 [123]	11.8 [123]	20-T_g				
	40	2.457 [123]	9.2 [123]	20-*T*				
	60	2.864 [123]	6.8 [123]	20-*T*				
	80	3.287 [123]	7.0 [123]	20-T_g				
	90	3.526 [123]	7.4 [123]					
Other metal oxides								
SnO	10					318 [151]	None up to 500 °C [151]	None up to 500 °C [151]
	20					351 [151]	None up to 500 °C [151]	500 °C [151]
	25					365 [151]	None up to 500 °C [151]	None up to 500 °C [151]
	40					384 [151]	None up to 500 °C [151]	None up to 500 °C [151]
	50					375 [151]	None up to 500 °C [151]	None up to 500 °C [151]
	60					360 [151]	None up to 500 °C [151]	None up to 500 °C [151]
	67					338 [151]	None up to 500 °C [151]	None up to 500 °C [151]
	75					325 [151]	None up to 500 °C [151]	None up to 500 °C [151]
PbO	1.9	1.960 [56]						
	3.5	2.050 [56]						
	7.6	2.315 [56]						

Table 3 continued

Oxide type ** second oxide	mol% second phase	Density ρ (g/cm^3)	Linear thermal expansion coefficient α (10^{-6} K^{-1})	Temperature range (°C)	Molar volume V_m (cm^3/mol)	Glass transition temperature T_g (°C)	Crystallization temperature (onset) T_x (°C)	Crystallization temperature (peak) T_p (°C)
	9	2.414 [56]						
	11	2.544 [56]						
	11.9	2.614 [56]						
	12.8	2.670 [56]						
	13.9	2.769 [56]						
	16.2	2.995 [56]						
	17.7	3.089 [56]						
	10							
	20					445 [153]		
	25							
	27					455 [153]		
		3.27 [126]				466 [152]; 487		650 [152]
	30	4.172 [130]				[130]	626.3 [152]	[130]
	33					452 [153]		
		5.06 [126]				450 [152]; 454		668 [152]
	40	4.964 [130]				[130]	647.5 [152]	[130]
	42					430 [153]		
		5.73 [126]				360 [152]; 400		
		5.73 [154];	10.2 (× 10^{-6} °C^1)			[153]; 339 [154]		
	50	5.677 [130]	[154]			406 [130]		551 [130]
	56					360 [155]		500 [155]
		6.19 [126]				328 [132]; 351		
	60	6.303 [130]				[130]		497 [130]
	65					320 [153]		
	70	6.86 [126]				2126 [152]	364.5 [152]	386 [152]
	80					292 [152]	355.3 [152]	360 [152]
		4.302 [156]						
	20	3.372 [157]	6.13 [156]	−100 to 150	33.40 [158]	469 [158]		564 [158]
	22.5	4.630 [156]	6.10 [156]	−100 to 150				
		4.815 [158]						
	25	4.873 [156]	6.32 [156]	−100 to 150	35.04 [158]	469 [158]	587 [158]	610 [158]
	27.5	5.136 [156]	6.52 [156]	−100 to 150				
		5.470 [158]						

Table 3 continued

Oxide type ** second oxide	mol% second phase	Density ρ (g/cm^3)	Linear thermal expansion coefficient α (10^{-6} K^{-1})	Temperature range (°C)	Molar volume V_m (cm^3/mol)	Glass transition temperature T_g (°C)	Crystallization temperature (onset) T_x (°C)	Crystallization temperature (peak) T_p (°C)
		5.379 [156]						
	30	4.010 [157]	6.66 [156]	−100 to 150	34.46 [158]	463 [158]	575 [158]	598 [158]
	32.5	5.614 [156]	6.160 [156]	−100 to 150				
	33	5.636 [158]			35.56 [158]	459 [158]	543 [158]	563 [158]
	35	5.834 [128]	6.93 [156]	−100 to 150				
		6.006 [158]						
		6.051 [156]				447 [158]; 447		547 [158]
	37.5	6.006 [141]	7.24 [156]	−100 to 150	36.34 [158]	[147]	529 [158]	[141]
		6.246 [156]						
		4.544 [157]				440 [158]; 437		540 [158]
	40	6.313 [149]	7.70 [156]	−100 to 150	36.14 [149]	[149]	513 [145]	[149]
		6.359 [158]						
	41	6.441 [156]	7.89 [156]	−100 to 150		433 [156]	509 [145]	533 [145]
	42	6.389 [145]			36.95 [145]	432 [145]	520 [145]	533 [145]
	47	6.737 [145]			37.98 [145]	414 [145]	484 [145]	4123 [145]
		6.874 [145]						
	50	5.273 [157]			38.96 [145]	408 [145]	439 [145]	424 [145]
	55	7.214 [145]			39.85 [145]	378 [145]	434 [145]	445 [145]
		7.550 [145]						
	60	5.977 [157]			40.72 [145]	358 [145]	411 [145]	429 [145]
	66	7.765 [145]			42.65 [145]	342 [145]	366 [145]	370 [145]
	70	6.705 [157]						
Lanthanide oxides								
La_2O_3	20	3.918 [18]						
	25	3.941 [18]						
	30	4.187 [18]						
CeO_2	20	3.04 [159]	21.6×10^{-6} °C−^{1} [159]	up to T_g	30.1 [159]	410 [159]		
	30	3.22 [159]	21.4×10^{-6} oC^1 [159]	up to T_g	30.5 [159]	423 [159]		
	40	3.62 [159]	21.0×10^{-6} °C−^{1} [159]	up to T_g	30.6 [159]	447 [159]		
	50	3.84 [159]	14.5×10^{-6} °C−^{1} [159]	up to T_g	31.7 [159]	467 [159]		
	55	3.54 [159]	10.0×10^{-6} °C^{-1} [159]	up to T_g	35.4 [159]	494 [159]		
	60	3.43 [159]	4.0×10^{-6} oC^1 [159]	up to T_g	37.2 [159]	523 [159]		
Pr_2O_3	20	4.122 [18]						

Table 3 continued

Oxide type ** second oxide	mol% second phase	Density ρ (g/cm^3)	Linear thermal expansion coefficient α (10^{-6} K^{-1})	Temperature range (°C)	Molar volume V_m (cm^3/mol)	Glass transition temperature T_g (°C)	Crystallization temperature (onset) T_x (°C)	Crystallization temperature (peak) T_p (°C)
	25	4.216 [18]						
	30	4.526 [18]						
Nd_2O_3	20	4.255 [18]						
	25	4.566 [18]						
	30	4.633 [18]						
Sm_2O_3	20	4.685 [18]						
	25	4.693 [18]						
	30	4.767 [18]						

Oxide type ** second oxide	mol% second phase	Melting temperatue (peak) T_m (°C)	Fraction of tetrahedral boron (N4)[a] N4	Dissolution rate and test temperature (g/cm^2 min); (°C)	Refractive index η	Young's modulus *E*GPa)	Bulk modulus *K*GPa)	Poisson's ratio ν
				3.8×10^{-3} (30 °C)				
Pure B_2O_3			0.0002 [124]	[125]	1.458 [123]			
Alkali metal oxides								
Li_2O	0.1							
	0.2							
	0.28					89.8 [126]		
	1					17.88 [127]	14.33 [127]	0.29 [127]
	5.0					21.85 [127]	15.26 [127]	0.26 [127]
				1.7×10^{-4} (30 °C)			18.26	
	10			[125]		26.01 [127]	[127]	0.26 [127]
	15					43.76 [127]	33.53 [127]	0.28 [127]
	17	771 ± 1 [129]						
	18	830 ± 2 [129]						
				4.3 × 10^{-}5 (30 °C)				
	20	836 ± 2 [131]		[125]				
	21	919 [124]						
	22	846 ± 6 [129]						
	24							
	25	872 ± 2 [129]						
	27	893 ± 4 [129]						

Table 3 continued

Oxide type ** second oxide	mol% second phase	Melting temperatue (peak) T_m (°C)	Fraction of tetrahedral boron (N4)[a] N4	Dissolution rate and test temperature (g/cm^2 min); (°C)	Refractive index η	Young's modulus *E*GPa)	Bulk modulus *K*GPa)	Poisson's ratio ν
	29	910 ± 6 [129]						
				2.8×10^{-5} (30 °C)				
	30			[125]				
	33.3							
	35							
	37.5		0.42 [134]					
	40			5.1×10^{-5} (30 °C) [125]				
	44.4		0.42 [134]					
	45							
	47.4		0.41 [134]					
			0.39 [134]; 0.38 [121]	7.1×10^{-5} (30 °C)				
	50			[125]				
	54.5		0.32 [134]					
	58.3		0.26 [134]					
	61.5		0.23 [127]					
	65		0.17 [134]					
	70		0.22 [121]					
	75							
Na_2O	5.4		0.04 [137]					
	8.7							
	10		0.12 [137]			29.0 [126]		
	10.21*							
	12							
	12.4		0.14 [137]					
	14.28*							
	15		0.18 [137]					
	16							
	17.4		0.22 [137]					
	17.5							
	18.3							
	19	800 [124]						
	20							
	20.16*							

Table 3 continued

Oxide type ** second oxide	mol% second phase	Melting temperatue (peak) T_m (°C)	Fraction of tetrahedral boron (N4)[a] N4	Dissolution rate and test temperature (g/cm^2 min); (°C)	Refractive index η	Young's modulus *E*GPa)	Bulk modulus *K*GPa)	Poisson's ratio ν
	22.1		0.30 [126]					
	23.7							
	24							
	25		0.30 [137]					
	25.7		0.351 [142]					
	25.99*							
	29.1		0.416 [142]					
	29.91*							
	30		0.38 [137]			47.8 [126]		
	32.5		0.41 [137]					
	33.3						45.9 [145]	
	33.7		0.434 [142]					
	33.8							
	35.0		0.43 [137]					
	35.8	742 [146]						
	35.94*							
	40							
	40.2		0.411 [142]					
	50							
	75							
K_2O	1.92		0.0201 [124]					
	4.05		0.0420 [124]					
	6.14		0.0618 [124]					
	8.23		0.0809 [124]					
	10.16		0.0963 [124]					
	12.27		0.1134 [124]					
	14.15		0.1284 [124]					
	16.1		0.1439 [124]					
	17.8		0.1590 [124]					
	19.8		0.1780 [124]					
	20							
	22.06		0.2033 [124]					
	25							

Table 3 continued

Oxide type ** second oxide	mol% second phase	Melting temperatue (peak) T_m (°C)	Fraction of tetrahedral boron (N4)[a] N4	Dissolution rate and test temperature (g/cm^2 min); (°C)	Refractive index η	Young's modulus *E*GPa)	Bulk modulus *K*GPa)	Poisson's ratio ν
	26	854 [124]	0.2554 [124]					
	28		0.2810 [124]					
	30							
	33.4							
	34.8	815 [146]						
	35							
	40							
	45							
	50							
Rb_2O	75							
	1.95		0.0207 [124]					
	4.05		0.0420 [124]					
	9.95		0.0914 [124]					
	14.99		0.1619 [124]					
	19.97		0.1656 [124]					
	22.49		0.1929 [124]					
	25		0.2246 [124]					
	29.95		0.2907 [124]					
	32.46		0.3140 [124]					
	37.47		0.3430 [124]					
	75							
Cs_2O	1.15		0.01168 [124]					
	2.18		0.02198 [124]					
	4.31		0.04344 [124]					
	8.61		0.07556 [124]					
	10							
	10.83		0.08929 [124]					
	14.94							
	18.65							
	20							
	22.72							
	25							
	26.32							

Table 3 continued

Oxide type ** second oxide	mol% second phase	Melting temperatue (peak) T_m (°C)	Fraction of tetrahedral boron (N4)[a] N4	Dissolution rate and test temperature (g/cm^2 min); (°C)	Refractive index η	Young's modulus *E*GPa)	Bulk modulus *K*GPa)	Poisson's ratio ν
	30.72							
	33							
	34.89							
	75							
Alkaline metal earth oxides								
MgO	16.7							
	23.1	1146 [148]						
	28.6	1146 [148]						
	33.3	1146 [148]						
	37.5	1146 [148]						
	44.4	1146 [148]						
	50.0							
	54.5							
	58.3							
CaO	9.1	971 [131]						
	16.7	971 [131]						
	20.0	971 [131]						
	23.1	971 [131]						
	25.0	971 [131]						
		971 [131]						
	25.9	971 [131]						
	26.3		0.329 [142]					
	28.6							
	29.8		0.367 [142]					
	30.0							
	33.3							
	33.5		0.394 [142]					
	35.0							
	40.0							0.279 [147]
	44.8							
	50.0		0.383 [142]					0.280 [147]
	55.0							
	58.3							

Table 3 continued

Oxide type ** second oxide	mol% second phase	Melting temperatue (peak) T_m (°C)	Fraction of tetrahedral boron (N4)[a] N4	Dissolution rate and test temperature (g/cm^2 min); (°C)	Refractive index η	Young's modulus *E*GPa)	Bulk modulus *K*GPa)	Poisson's ratio ν
	60.0							0.280 [147]
	70.0							0.297 [147]
		940 [135]						
SrO	5.0	988 [135]						
		940 [135]						
	9.1	988 [135]						
		940 [135]						
	16.7	988 [135]						
	28.6							
	33.3							
	37.5							
	44.4							
	50.0							
	54.5							
	61.5							
	64.5							
BaO	9.1	878 [131]						
	16.7	878 [131]						
	23.1							
	25.6		0.341 [142]					
	28.6							
	29.6		0.0.395 [142]					
	33.3							
	34.4		0.431 [142]					
	37.5							
	39.6		0.445 [142]					
	44.4							
	47.4							
	50.4		0.359 [142]					
	63.0							
	64.3							
	65.5							
Transition metal oxides								

Table 3 continued

Oxide type ** second oxide	mol% second phase	Melting temperatue (peak) T_m (°C)	Fraction of tetrahedral boron (N4)[a] N4	Dissolution rate and test temperature (g/cm^2 min); (°C)	Refractive index η	Young's modulus *E*GPa)	Bulk modulus *K*GPa)	Poisson's ratio ν
ZnO	60.0							
GeO	5				1.480 [123]			
	10				1.502 [123]			
	15				1.516 [123]			
	20				1.531 [123]			
	40				1.562 [123]			
	60				1.579 [123]			
	80				1.598 [123]			
	90				1.604 [123]			
Other metal oxides								
SnO	10							
	20							
	25							
	40		0.26 [151]					
	50		0.28 [151]					
	60							
	67		0.25 [151]					
	75							
PbO	1.9							
	3.5							
	7.6							
	9							
	11							
	11.9							
	12.8							
	13.9							
	16.2							
	17.7							
	10	656.0 [152]						
	20	673.2 [152]						
	25		0.26 [69]					
	27							
		728 717.2 [152]	0.32 [69] 0.35					

Table 3 continued

Oxide type ** second oxide	mol% second phase	Melting temperatue (peak) T_m (°C)	Fraction of tetrahedral boron (N4)[a] N4	Dissolution rate and test temperature (g/cm^2 min); (°C)	Refractive index η	Young's modulus *E*GPa)	Bulk modulus *K*GPa)	Poisson's ratio ν
	30	798 [130]	[130]	3.78 (90 °C) [39]		59.3 [126]		
	33							
		576 703.6 [152]	0.4 [69]; 0.43					
	40	671 [130]	[130]	2.18 (90 °C) [39]		64.1 [126]		
	42							
		537.0 [152]	0.47 [154]; 0.43					
	50	598 [130]	[69]; 0.45 [130]	3.08 (90 °C) [39]		60.3 [126]		
	56	600 [155]						
		522.1 [152]	0.33 [69]; 0.39					
	60	566 [130]	[130]	0.11 (90 °C) [39]		49.6 [126]		
	65							
	70	469.1 [152]	0.2 [69]	0.04 (90 °C) [39]		41.0 [126]		
	80	457 [152]	0.12 [69]	0.03 (90 °C) [39]				
	20	678 [158]	0.323 [158]					
	22.5							
	25	678 [158]	0.358 [158]					
	27.5							
	30	676 [158]	0.409 [158]					
	32.5							
	33	674 [158]	0.427 [158]					
	35							
		547 728 [158]						
	37.5	728 [141]	0.444 [158]					
		544 648 [158]						
	40	650 [149]	0.454 [158]					
	41	650 [145]	0.451 [145]					
	42	643 [145]	0.460 [145]					
	47	651 [145]	0.447 [145]					
	50	653 [145]	0.454 [145]					
	55	652 [145]	0.419 [145]					
	60	650 [145]	0.388 [145]					
	66	680 [145]	0.314 [145]					

Table 3 continued

Oxide type ** second oxide	mol% second phase	Melting temperatue (peak) T_m (°C)	Fraction of tetrahedral boron (N4)[a] N4	Dissolution rate and test temperature (g/cm^2 min); (°C)	Refractive index η	Young's modulus *E*GPa)	Bulk modulus *K*GPa)	Poisson's ratio ν
	70							
Lanthanide oxides								
La_2O_3	20							
	25							
	30							
CeO_2	20							
	30							
	40							
	50							
	55							
	60							
Pr_2O_3	20							
	25							
	30							
Nd_2O_3	20							
	25							
	30							
Sm_2O_3	20							
	25							
	30							

Significant figures are given in the table as reported in the original reference or as approximated from graphs

* Experimental composition

** Classification based on Ref. [160]

[a] For theoretical models of N4, the reader is referred to original and modified Dell and Bray models [161–164]

Table 4 Glass stability parameters calculated for various borate glasses

Second oxide	mol% Second phase	Weinberg parameter K_w	Hrubÿ parameter K_H	Lu–Liu parameter K_{LL}
Li_2O	**17**	**0.19**	**0.60**	**0.47**
	18	0.15	0.37	0.44
	20	0.11	0.28	0.43
	22	0.09	0.23	0.42
	25	0.09	0.25	0.42
	27	0.09	0.22	0.41
	29	0.09	0.18	0.40
PbO	30	0.26	1.76	0.53
	40	**0.31**	**3.52**	**0.56**
	56	0.23	*	*
	70	0.18	0.49	0.46
	80	0.15	0.56	0.47
Bi_2O_3	20	0.14	*	*
	25	**0.28**	**1.30**	**0.51**
	30	0.20	1.11	0.50
	33	0.15	0.64	0.48
	37.5	0.14	0.41	0.47
	40	0.15	0.54	0.47
	41	0.15	0.54	0.48
	42	0.16	0.72	0.48
	47	0.12	0.42	0.45
	50	0.03	0.14	0.41
	53	0.08	0.20	0.42
	55	0.10	0.26	0.42
	60	0.11	0.22	0.41
	66	0.04	0.08	0.36

Bold numbers indicate the highest glass stability parameters in each data set

* Literature data for calculations not available

earth oxide content. The glass formation range is very broad in the case of PbO–B_2O_3 and Bi_2O_3–B_2O_3 systems. Furthermore, liquidus temperatures are quite low (Table 3). Both of these conditions make it convenient to make glass in these systems. In the case of alkali borate systems, on the other hand, liquidus temperatures rise rapidly with increasing alkali oxide content. So, most of the alkali borate compositions have melting points similar to silicate or borosilicate glasses [81].

Two possible routes to phase separation in glasses are stable and metastable phase separation. Stable phase separation will occur if the phase diagram of the glass-forming system contains a region of liquid–liquid immiscibility above the liquidus temperature and if the glass composition corresponds to this region. Cooling from this region will result in two separate phases in the final product. Many binary borate systems exhibit such stable phase separation, including Bi_2O_3–B_2O_3 [82], BaO–B_2O_3 [83], Nb_2O_5–B_2O_3 [84] and La_2O_3–B_2O_3 [85]. The phase equilibrium diagram for the system BaO–B_2O_3 is shown in Fig. 7 as an example, indicating the region of stable immiscibility, the upper consolute (critical) temperature, T_c, and corresponding critical composition, θ_c. Interestingly, in most such systems, the region of immiscibility occurs in the B_2O_3 rich side of binary phase diagrams. The PbO–B_2O_3 system also exhibits stable phase separation [86]. The immiscibility region lies between 0.4 and 20 mol% PbO [87]. This is one of the commonly studied systems regarding immiscibility because the phase separated regions have a big difference in terms of density, which facilitates microstructural analysis. Zhu et al. [88] studied the microstructure of phase separated lead borate glasses prepared under low gravity. Figure 8 shows the resulting microstructure in $3.5PbO–96.5B_2O_3$ glass. The microstructure is composed of a continuous borate-rich phase in which lead-rich droplets are distributed. It was reported that the addition of a small amount (e.g., 4 mol%) of Al_2O_3 reduces phase separation in the PbO–B_2O_3 system [89].

Table 5 Ranges of glass formation and phase separation in binary borate systems

Oxide type*	Second oxide	Glass formation range (mol% second oxide)		Immiscibility range (mol%) at T_{mo}** or T_{arb}	Upper consolute (critical) temperature for phase separation T_c (°C)	Critical composition for phase separation $_{\theta c}$ (mol fraction)	Glass-forming method	Approximate cooling rate
		First range	Second range					
Alkali metal oxides								
	Li_2O	0.050.0 [130, 165]		3.015.0 [166]	453 [167]; 660 [90]	0.045 [167]; 0.10 [90]	Press quenching [165]	10^2–10^3 K/s
	Na_2O	0.050.0 [25, 151]	66.571.5 [131, 151]				Press quenching [151]	10^2–10^3 K/s
		0–46 [168]	54–76 [168]				Roller quencher [168]	10^5 °C/s
	K_2O	0.050.0 [25, 151]					Press quenching [151]	10^2–10^3 K/s
	Rb_2O	0.0–44.5 [169]	65.5–73.0 [169]				Hammer and anvil [169]	
	Cs_2O	0.0–46.5 [169]	57.5–73.0 [169]				Hammer and anvil [169]	
Alkaline metal earth oxides								
	MgO	1.0–49.2 [170]		1.0–49.2 (1142 °C) [170]	1770 ± 200 [171]	0.14 ± 0.02 [171]	Cooled in Pt crucible in air [170]	
	CaO	28.041.0 [26]		1.0–27.0 (971 °C) [172]	1515 ± 100 [171]	0.08 ± 0.01 [171]		
		20.0–70.0 [147]					Melt quenching [147]	
	SrO	24.0–43.0 [149]		1.0–19.0 (1038 °C) [172]; 1.0–10.0 (1050 °C) [173]	1390 ± 50 [173], 1435 [171]	0.06 ± 0.02 [173], 0.08 [171]		
				1–33 (910 °C) [131]				
	BaO			1.0–16.5 (878 °C) [172]; 3.5–12.0 (1100 °C) [173]	1180 [173], 1256 [171], 1150 ± 10 [174]	0.074 [173], 0.075 [175], 0.055 [171], 0.070 ± 0.005 [173]		
		16.766.7 [121, 149]		0–16.7 (NA) [130]			Roller quenching [130]	10^5 °C/s
				1–20 (878 °C) [131]				
Transition metal oxides								
	CoO			2–55 (1050 °C) [131]				
	ZnO	44.0–63.0 [25]		1.050.0 (998 °C) [7, 131, 170]			Pouring on steel plate [150]; cooled in Pt crucible in air [170]	

Table 5 continued

Oxide type*	Second oxide	Glass formation range (mol% second oxide)		Immiscibility range (mol%) at T_{mo}** or T_{arb}	Upper consolute (critical) temperature for phase separation T_c (°C)	Critical composition for phase separation $_{\theta c}$ (mol fraction)	Glass-forming method	Approximate cooling rate
		First range	Second range					
	Nb_2O_5	No homogeneous glass was obtained—all samples devitrified [84]		10–65.7 (1352 °C) [84]				
	Ag_2O	0.0–33.0 [24]					Melt quenching [24]	
	CdO			2–40 (978 °C) [131]				
Metalloid oxides								
	SiO_2	0.0100.0 [25, 169]		subliquidus	520 [91]	0.5 [91]	Hammer and anvil [169]	
	GeO_2	0.0–100.0 [123]; 0–100 [176]						
	TeO_2			26–95 (680 °C) [177]	1198 [177]	60 [177]		
Non-metal oxides								
	P_2O_5	Not compatible (melts crystallize or phase separate when quenched) [95]						
Other metal oxides								
	SnO	0.0–75.0 [151] 0–80 [165]					Press quenching [151]	10^2–10^3 K/s
	Tl_2O	0.0–45.0 [25]						
	PbO	20.0–80.0 [25, 101]; 22–85 [176]		0.4–20 (800°) [87]; 3–17 (745 °C) [178]; 1–19.4 (600 °C) [97]; 5–42 (700 °C) [179]; 0.7–19.5 (600 °C) [180]	800 [131]; 785 [178]; 784.1 [179]; 790 [179]	0.1 [178]; 0.1 [179]; 4–12*** [179]	Press quenching [101]; Cooled in Pt crucible in air [178]	102–103 K/s [101]; 20 °C/min [178]
	Bi_2O_3	7.7–80.0 [145]		0–19.0 (709 °C) [82]	831 [78]			
Lanthanide oxides								
	La_2O_3	22.0–27.0 [7]		0–21.5 (1136 °C) [85]				

Significant figures are given in the table as reported in the original reference or as approximated from graphs

* Classification based on [160]

** Range of phase separation at designated monotectic temperature T_{mo} or at an arbitrary temperature

*** Flat top, no peak

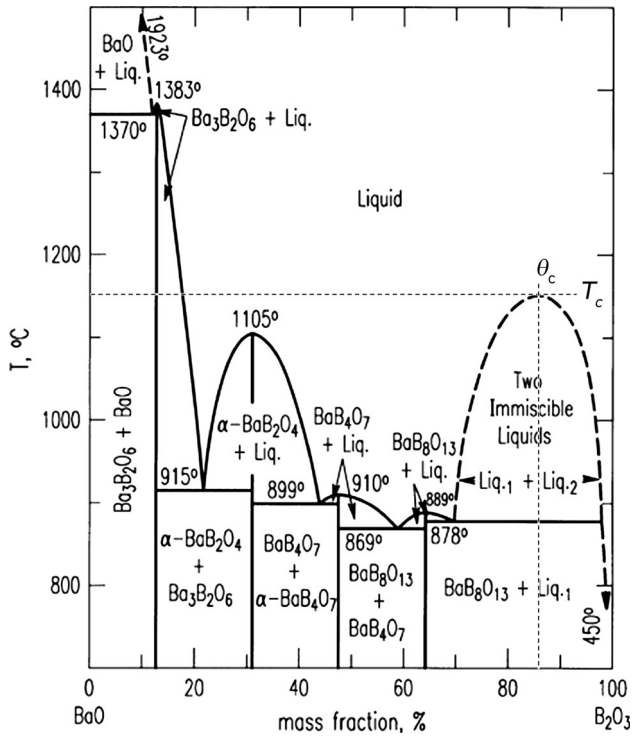

Fig. 7 Phase diagram of the binary system $BaO–B_2O_3$ (Adapted from Ref. [114])

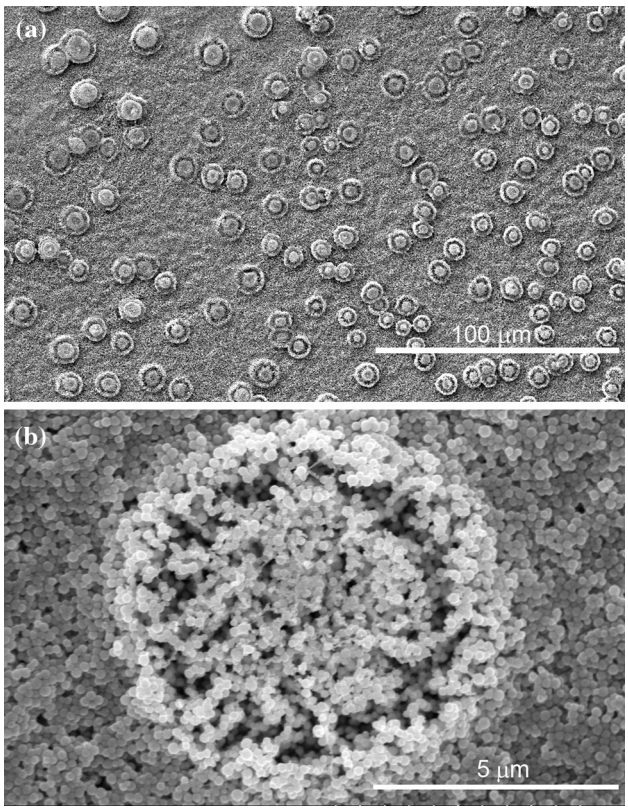

Fig. 8 **a** SEM micrograph of phase separated $3.5PbO·96.5B_2O_3$ glass and **b** detail of lead-rich phase (Courtesy of Dongmei Zhu, State Key Laboratory of Solidification Processing, Northwestern Polytechnical University, Xi'an, Shaanxi 710072, People's Republic of China)

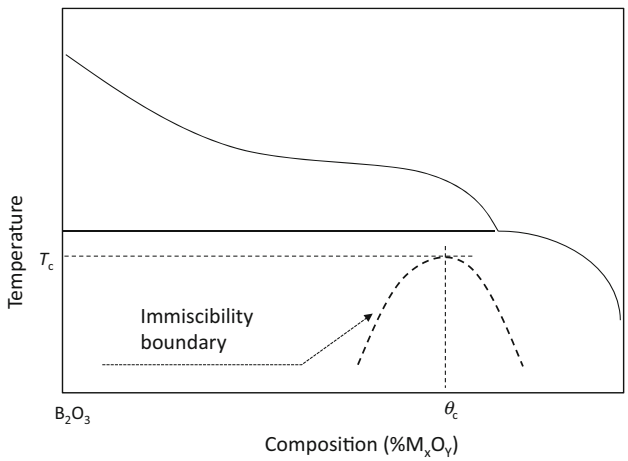

Fig. 9 Hypothetical phase diagram with a region of subliquidus immiscibility

The second route for phase separation in glasses is metastable, which occurs below the liquidus temperature. Figure 9 shows a typical phase diagram with a region of metastable or subliquidus immiscibility. Such diagrams are useful to predict the type of microstructure (isolated droplets or interconnected phases) based on the composition and quenching rate [1]. Two binary borate systems known to exhibit metastable immiscibility are $Li_2O–B_2O_3$ [90] and $B_2O_3–SiO_2$ [91]. Although it was claimed in the 1960s that other alkali borate systems including $Na_2O–$, $K_2O–$, $Rb_2O–$, and $Cs_2O–B_2O_3$ also exhibit metastable immiscibility [90], later studies suggested that no miscibility gaps existed or no phase separation occurred in them [92, 93]. Yet electron microscopy imaging provided proof of phase separation at the nanoscale in sodium borate glasses [94]. Du et al. [95] found that it takes long time in $15Na_2O–86B_2O_3$ glass to reach equilibrium during phase separation. At 500 °C, 20 h of heat treatment was necessary to fully convert glass samples to $Na_2O·9B_2O_3$ and $3Na_2O·B_2O_3$. The long time for reaching equilibrium was attributed to the difficulty in crystallizing the Na-rich phase due to overcoordination of oxygen atoms during conversion of some trigonal borates to tetrahedral borates. Binary immiscibility diagrams are not well established and controversy remains in many borate or silicate systems. It is also questioned whether immiscibility in the $B_2O_3–SiO_2$ system exists [1]. Further study would be very valuable to clarify the question of immiscibility. New tools and techniques need to be applied for more reliable results.

Although normally undesirable, phase separation has, in some cases, been used to obtain unique materials such as porous, anisotropic, and nonlinear optic glasses [96]. For

example, in the Vycor® process, a microporous glass with a composition of nearly pure SiO_2 is obtained by leaching the alkali borate phase from the interconnected silica-borate structure [94]. It is essential to know the phase separation rate or the nucleation and growth rates in the systems of interest for optimum results when making practical use of phase separation. Some experimental results exist for $BaO–B_2O_3$ and $PbO–B_2O_3$ systems in this regard [88, 94, 97].

Chemical durability

So far, binary borate, particularly alkali and alkaline earth borate glasses could find no practical application since their chemical durability is unacceptably low. Table 6 gives a better idea of how their chemical durability compare with those of other glasses. Industrially useful levels of chemical durability have been obtained in CaO-aluminoborate (CaBAl) glasses developed for sealing applications [98]. The chemical durability of CaBAl glasses in water at 70–90 °C is in the order of 10^{-6} g/(cm^{2}min) [99, 100]. However, the melting point of CaBAl glasses are higher than many binary borate glasses; for example that of CaBAl17 ($50CaO{\cdot}30B_2O_3{\cdot}20Al_2O_3$) is 940 °C [100].

Studies in the $PbO–B_2O_3$ system showed that the chemical durability of glasses in this system is much better compared to alkali borate ($Na_2O–B_2O_3$) or alkaline earth borate ($CaO–B_2O_3$) glasses. The aqueous dissolution rate of lead borate glasses at 90 °C is five to six orders of magnitude smaller compared to $Na_2O–B_2O_3$ glasses (Table 6). The chemical durability of glasses in the $PbO–B_2O_3$ system increases as the PbO content increases. This increase is not linear but there seems to be some compositional ranges where the dissolution mechanism remains the same. In the first compositional range where PbO = 30–50 mol% and B_2O_3 = 70–50 mol%, the dissolution rate is 2–3 × 10^{-6} g/(cm^{2}min) (Table 6). The aqueous dissolution rate of $60PbO.40B_2O_3$ glass is ~2 × 10^{-7} g/(cm^{2}min). Lead borate glasses with high (70–80 mol%) PbO content exhibit the lowest dissolution rate, namely ~3.6 × 10^{-8} g/(cm^{2}min) in this system. The

Table 6 Dissolution rates of various glasses in water

Glass type	Composition (mol%)	Test water temperature (°C)	Dissolution rate g/(cm^2 min)	References
Pure borate glass	B_2O_3	30	3.8 × 10^{-3}	[125]
Lithium borate	$Li_2O–3B_2O_3$ + 5 wt%SiO_2	25	7.9 × 10^{-6}	[129]
Lithium borate	$30Li_2O–70B_2O_3$	30	2.7 × 10^{-5}	[129]
Sodium borate	$30Na_2O–70B_2O_3$	90	1.1 × 10^{-3}	[102]
Calcium borate	$35CaO–65B_2O_3$	90	4.7 × 10^{-6}	[102]
Lead borate	$30PbO–70B_2O_3$	90	3.0 × 10^{-6}	[102]
Lead borate	$40PbO–60B_2O_3$	90	1.9 × 10^{-6}	[102]
Lead borate	$50PbO–50B_2O_3$	90	2.8 × 10^{-6}	[102]
Lead borate	$60PbO–40B_2O_3$	90	2.1 × 10^{-7}	[102]
Lead borate	$70PbO–30B_2O_3$	90	3.7 × 10^{-8}	[102]
Lead borate	$75PbO–25B_2O_3$	90	3.7 × 10^{-8}	[102]
Lead borate	$80PbO–20B_2O_3$	90	3.5 × 10^{-8}	[102]
Pb–Zn borophosphate	$25PbO–25ZnO–15B_2O_3–35P_2O_5$	100	1.2 × 10^{-6}	[181]
Barium aluminoborate (BaBAl)	$29.4BaO–49B_2O_3–19.6Al_2O_3–2Fe_2O_3$	90	9.3 × 10^{-7}	[182]
Calcium borophosphate	$0.8Ca(PO_3)_2–0.2B_2O_3$	25	6.7 × 10^{-7}	[183]
Borosilicate (CVS-IS)	$53.3SiO_2–10.5B_2O_3–11.3Na_2O–2.4Al_2O_3–3.7Li_2O–7.0Fe_2O_3–3.9ZrO_2–1.3Nd_2O_3$ and 6.6 % others (wt%)	90	2.6 × 10^{-8}	[184]
Aluminosilicate (CVS-IS)	$55.9SiO_2–5.0B_2O_3–20.0Na_2O–12.0Al_2O_3–4.0CaO$ and 3.1 % others (wt %)	90	8.8 × 10^{-9}	[184]
Calcium aluminoborate (CaBAl)	$30CaO–40B_2O_3–30Al_2O_3$	70	9.9 × 10^{-7}	[99]
Calcium aluminoborate (CaBAl)	$50CaO–30B_2O_3–20Al_2O_3$	90	1.3 × 10^{-6}	[100]
$SrTiO_3$–aluminoborate	$15SrO–15TiO_2–47B_2O_3–23Al_2O_3$	90	2.1 × 10^{-7}	[100]
$SrTiO_3$–aluminoborate + P_2O_5	$15SrO–15TiO_2–42B_2O_3–19Al_2O_3–9P_2O_5$	90	1.4 × 10^{-9}	[100]

addition of 5 mol% PbO reduces the dissolution rate of $30Na_2O{\cdot}70B_2O_3$ by about two orders of magnitude. The relatively high chemical durability in borate glasses with 5–50 mol% can be explained by a high content of BO_4 groups in the glass network. On the other hand, the significantly high chemical durability in borate glasses with more than 50 mol% PbO can be explained by an increased covalency of Pb–O bonds where PbO acts a network former [4, 101].

The addition of small amounts of P_2O_5 to $SrTiO_3$-aluminoborate glasses resulted in aqueous dissolution rates of about two orders of magnitude lower than found in the original glasses. This unexpected improvement in chemical durability was attributed to the replacement of BO_3 units by chemically resistant BO_4 units [100]. Subsequent studies investigated whether P_2O_5 additions could improve the chemical durability of simpler borate glasses. However, such an effect could not be observed in binary systems. For example, the aqueous dissolution rate of $30Na_2O.70B_2O_3$ at 90 °C did not decrease but rather increase from $\sim 1\times10^{-3}$ to 2×10^{-3} g/(cm^2 min) with 5–20 mol% P_2O_5 additions [102].

A comparative analysis of aqueous dissolution rates of various borate and other types of glass (Table 6) leads to the following comments:

- In general, simple alkali- or alkaline earth-borate glasses possess very low chemical durability.
- On the other hand, some complex borate glasses such as $SrTiO_3$–B_2O_3–P_2O_5 glasses have comparable chemical durabilities to borosilicate glasses.
- Lead borate glasses with high lead content possess comparable chemical durability to borosilicate glasses. The former glasses are simple to make and have very low melting temperatures. Unfortunately, they are not suitable for applications such as biomedical fields due to the toxicity of lead. However, they are good candidates for innovative applications where toxicity is not a major issue.

Factors related to borate melts and potential implications on glass properties

Commercial or experimental glass making requires close control of process parameters and environmental factors for optimized and consistent results. Some factors commonly known to influence the quality of glass products are melting temperature, cooling rate, batch volume, annealing schedule, purity of raw materials, gas evolution from raw materials, volatilization of components, and mixing of the melt [1].

One of the attractive features of borate glasses is their considerably lower melting and processing temperatures, in the absence of silica or other refractory oxides. The melting temperature depends on the composition and purity. Melting temperatures of binary alkali borate glasses range between ~500 and 920 °C (Table 3). Among various glass-forming xR_2O–yB_2O_3 compositions, the maximum melting temperatures and corresponding amounts of R_2O are 919 °C & 21 mol% for Li_2O; 854 °C & 26 mol% for K_2O, and 800 °C & 19 mol% for Na_2O [2]. Alkaline earth borate glasses have typically higher melting points, ranging from ~880 to 1150 °C. The melting temperatures for binary PbO–B_2O_3 glasses range between ~470 and 720 °C, while those of Bi_2O_3–B_2O_3 range between ~650 and 730 °C.

In the glass transition region, addition of alkali oxides increases the viscosity until a maximum is reached at about 20–30 mol% R_2O. Further additions decrease the viscosity monotonically. Therefore, a viscosity-% R_2O curve creates a parabola with a maximum point. Viscosity curves for Sb_2O_3–B_2O_3 and Bi_2O_3–B_2O_3 melts exhibit very similar behavior to R_2O–B_2O_3 melts. In R_2O–B_2O_3 melt systems, the increase in viscosity up to the maximum has been interpreted as an increase of connectivity in the melt network through the destruction of boroxol rings and formation of $BO_{4/2}R$ tetrahedra. Above the maximum, increased fluidity occurs due to non-bridging oxygen atoms in $BO_{n/2}(OR)_{(3-n)}$ triangles ($n = 1,2,3$) [103]. According to these observations, glasses in alkali oxide-borate systems should be selected sufficiently far from 20 to 30 mol% alkali oxide compositions in order to obtain melts with lower viscosity for practical reasons. If, for any reason, 20–30 mol% alkali oxide is preferable in a borate glass, higher temperatures ($T > 1000$ °C) could be used for casting.

In the case of B_2O_3–SiO_2 and B_2O_3–GeO_2 systems, the transition range viscosity increases monotonically with increasing SiO_2 or GeO_2 content. The monotonic increase has been explained by the splitting of boroxol rings into individual $BO_{3/2}$ triangles which are linked to $SiO_{4/2}$ (Q4) or $GeO_{4/2}$ tetrahedra [1, 103].

Gases released from decomposition of carbonates, nitrates, and sulfates, or from the evaporation of moisture absorbed on particles can lead to bubbles. Small amounts of fining agents are added to the batch to reduce bubble formation. Even though most borate glasses have lower viscosities than silica glasses, bubble entrapment can still be a problem in them. As_2O_3 and Sb_2O_3 are the most efficient fining agents but they are toxic. Nitrates can be used instead of these toxic agents but they have low decomposition temperatures ranging from 500 to 800 °C. While they are not preferred for silica glasses, they may be suitable for low melting temperature borate glasses. CeO_2

is an acceptable substitute for As_2O_3 and Sb_2O_3 at higher melting temperatures.

Another potential problem in borate glasses is entrapped H_2O. Recent studies confirmed that the solubility of water is much greater in borate melts compared to silica melts. The solubility was measured as 5600–6500 ppm (mass/mass) of H_2O at 800 °C and 6400–6900 ppm at 900 °C in alkali borate melts, whereas the highest solubility for comparable silica melts is about 2300 ppm. The solubility of water in alkali borate melts was shown to decrease by a factor of two or more as the alkali oxide concentration increased from 0 to 40 mol%. The large amount of water in borate glasses results in a wide spread of glass transformation temperature values [104, 105]. Water dissolved in the melt tends to react with oxide glasses and cause a replacement of bridging oxygen atoms by hydroxyl groups. Such reactions result in weaker network connectivity, lower glass transformation temperatures, lower viscosities, and higher crystallization rates, in general [105].

Volatilization of borate species from glass melts is an important phenomenon to consider in glass making or high-temperature applications such as sealing. Volatile species responsible for weight loss were determined to be mainly BO_2 (g) in dry conditions and $B_3H_3O_6$ (g) in wet, reducing conditions [106]. Major (up to 20 %) weight losses have been found to occur at melting temperatures or above when borate was the only network former in the glass composition [107]. Studies with B_2O_3-containing glasses indicated that the amount of boron volatilization increases with the melting temperature, partial water pressure in the melting environment, and B_2O_3 fraction in the glass [106, 108]. Volatilization of borate species has to be kept under control because it would affect all glass properties. For example, the density and refractive index of E-glass increased as the boron content of glasses decreased [108].

Khanna et al. demonstrated that the properties of lead borate and bismuth borate glasses can vary significantly with melt annealing [109, 110]. The density and elastic modulus decreased while the glass transition temperature increased with increasing melt aging time (i.e., the duration of annealing at a given temperature above liquidus) in a bismuth borate glass with the composition $40Bi_2O_3$–$60B_2O_3$. Similar results were obtained in PbO–B_2O_3 of various compositions [109]. In the case of bismuth borate glass, increasing the aging time from 15 to 220 min decreased the density from 5.84 to 4.97 g/cm^3 and the longitudinal modulus from 86.3 to 80.3 GPa, while it increased T_g from 455 to 474 °C, respectively [110]. No selective evaporation of constituents from the melt was detected. Property changes were attributed to structural rearrangement of the melt from a high density amorphous to a low density amorphous state due to the structural transformation,

$$B\emptyset_4^- \Rightarrow B\emptyset O^-, \quad (10)$$

where $\emptyset$ represents a bridging oxygen while O^- refers to a non-bridging oxygen. Time related effects were also reported for lithium tetraborate and sodium tetraborate melts but the change in glass density was only in the order of 3 % [111, 112]. The melt aging effect may be one of the reasons for significant variations in properties of binary borate glasses with the same nominal composition (Table 3). It was suggested that various properties of heavy metal oxide borate glasses can be tailored by changing the aging time of the corresponding melt without altering the composition or quenching rate [110]. More detailed analysis of melt aging effects on different glass properties would be valuable both for scientific and industrial reasons.

Implications for future research and applications

Various non-silicate borate glasses have been developed for applications where silica chemistry is not suitable or where the borate network offers certain advantages over silica or other types of glasses. While the unique structure and chemistry of borate glasses offers important advantages and possibilities, certain deficiencies such as low chemical durability necessitate the formulation of carefully selected compositions. This review discussed binary borate glasses in general. Among binary borates, lead borate systems offer certain advantages such as good chemical durability and low processing temperatures. However, the toxicity of lead will gradually restrict the applications of lead borate glasses due to regulations and environmental concerns. The low toxicity of bismuth makes it a candidate for replacement of lead in low melting point solders [113]. Similarly, bismuth borate glasses may be preferable for sealing and other applications that require low melting points. Typically, ternary and more complex borate glasses are needed for advanced applications. The effort of choosing the right composition requires a good analysis of the scientific literature available on the subject. The literature and collected data for similar compositions (Table 3) indicate that there is considerable variability in reported experimental data. Reasons for such variability may include H_2O dissolved in the glass network in the form of hydroxyl groups, melt aging, and experimental errors inherent in related testing and measurement equipment. The appreciation and minimization of such factors is a necessity for better control of glass preparation and resulting properties.

Although research on borate glasses dates back to more than a century ago, some basic investigations such as the

development of phase diagrams of binary systems may be worthwhile repeating with more sophisticated experimental tools and thermodynamic calculations since the reliability of some older data is now under debate. For example, as mentioned earlier in this review, regions of immiscibility for alkali borate systems are still not well defined. Another important contribution to the study of borate glasses would be related to chemical durability. Data on the chemical durability of borate glasses in different media (water, acidic, basic, etc.) are quite limited and difficult to compare. While some standard testing methods exist, they are relatively complicated. Development of simple standards for chemical durability testing seems to be an important necessity. The effect of various factors such as water content and melt aging on glass properties is another field where further research would be valuable. Relatively new approaches such as computerized simulation would be useful for predicting long-term effects such as leaching from waste glasses in underground storage areas or volatilization of borate from sealing glasses used at elevated temperatures.

References

1. Shelby JE (2015) Introduction to glass science and technology. Royal Society of Chemistry, Cambridge
2. Bobkova NM (2003) Thermal expansion of binary borate glasses and their structure. Glass Phys Chem 29:501–507
3. Rachkovskaya GE, Zakharevich GB (2002) Vitrification, properties, and structure of lead-tellurite borate glasses. Glass Ceram 59:123–126
4. Cheng Y, Xiao H, Guo W (2007) Influence of compositions on sealing temperature and properties of lead borate non-crystallizing sealing glasses. Mater Sci Eng, A 464:210–215
5. Koudelka L, Mošner P, Zeyer M, Jäger C (2003) Lead borophosphate glasses doped with titanium dioxide. J Non-Cryst Solids 326:72–76
6. Brochu M, Gauntt BD, Shah R, Loehman RE (2006) Comparison between micrometer-and nano-scale glass composites for sealing solid oxide fuel cells. J Am Ceram Soc 89:810–816
7. Brow RK, Tallant DR, Crowder SV, Saha SK, Jain H, Mcintyre A, Day DE (1996) Advanced materials for aerospace and biomedical applications. Sandia Report, Albuquerque, pp 96–2772
8. Bowers B (2002) Discharge lighting brightens the night. Proc IEEE 90:1604–1607
9. Laughton MA, Warne DF (eds) (2003) Electrical engineer's reference book. Elsevier, Oxford
10. Linden D, Reddy T (2001) Handbook of batteries. McGraw-Hill, New York
11. Sudworth J, Tilley AR (1985) Sodium sulfur battery. Chapman and Hall, London
12. Rahmane M, Lacovangelo C (2010) Materials for advanced sodium metal halide batteries, leadership summit. American Ceramic Society, Baltimore
13. Wikipedia (2011) Lithium battery. http://en.wikipedia.org/wiki/Lithium_battery. Accessed 11 June 2015
14. Fusite Corporation (2011) Hermetic glass to metal battery seals booklet. http://www.emersonclimate.com/Documents/Battery.pdf. Accessed July 28 2011
15. Brow RK, Tallant DR (1997) Structural design of sealing glasses. J Non-Cryst Solids 222:396–406
16. Schaffer JP, Saxena A, Antolovich SD, Sanders TH Jr, Warner SB (1999) The science and design of engineering materials. McGraw-Hill International, New York
17. Brow RK and Watkins RD (1991) U.S. Patent No. 5,021,307. U.S. Patent and Trademark Office, Washington, DC
18. Volf MB (1990) Technical approach to glass. Elsevier, Amsterdam
19. Pecht M, Fukuda Y, Rajagopal S (2004) The impact of lead-free legislation exemptions on the electronics industry. IEEE Trans Electron Packag Manuf 27:221–232
20. Aitken BG, Bookbinder DC, Greene ME, Morena RM (1993) U.S. Patent No. 5,246,890. U.S. Patent and Trademark Office, Washington, DC
21. Francis GL, Morena R (1994) US Patent No. 5,281,560. U.S. Patent and Trademark Office, Washington, DC
22. Woods WG (1994) An introduction to boron: history, sources, uses, and chemistry. Environ Health Perspect 102(Suppl 7):5
23. Terashima K, Tamura S, Kim SH, Yoko T (1997) Structure and nonlinear optical properties of lanthanide borate glasses. J Am Ceram Soc 80:2903–2909
24. Yamane M (2000) Glasses for photonics. Cambridge University Press, Port Chester
25. Harper CA (2001) Handbook of ceramics, glasses and diamonds. McGraw-Hill, New York
26. Qiu J, Tanaka N, Sugimoto N, Hirao K (1997) Faraday effect in Tb^{3+}-containing borate, fluoride and fluorophosphates glasses. J Non-Cryst Solids 213&214:193–198
27. Gan F (ed) (2006) Photonic glasses. World Scientific, River Edge
28. Nie W (1993) Optical nonlinearity: phenomena, applications, and materials. Adv Mater 5:520–545
29. Deparis O, Mezzapesa FP, Corbari C, Kazansky PG, Sakaguchi K (2005) Origin and enhancement of the second-order non-linear optical susceptibility induced in bismuth borate glasses by thermal poling. J Non-Cryst Solids 351:2166–2177
30. Nazabal V, Fargin E, Ferreira B, Le Flem G, Desbat B, Buffeteau T, Couzi M, Rodriguez V, Santran S, Canioni L, Sarger L (2001) Thermally poled new borate glasses for second harmonic generation. J Non-Cryst Solids 290:73–85
31. Boyd RW, Fischer GL (2001) Nonlinear optical materials. In: Buschow KHJ et al (eds) Encyclopedia of materials: science and technology. Elsevier, New York
32. Myers RA, Mukherjee N, Brueck SRJ (1991) Large second-order nonlinearity in poled fused silica. Opt Lett 16:1732–1734
33. Corbari C, Ajitdoss LC, Carvalho ICS, Deparis O, Mezzapesa FP, Kazansky PG, Sakaguchi K (2010) The problem of achieving high second-order nonlinearities in glasses: the role of electronic conductivity in poling of high index glasses. J Non-Cryst Solids 356:2742–2749
34. Akselrod MS, Bøtter-Jensen L, McKeever SWS (2007) Optically stimulated luminescence and its use in medical dosimetry. Radiat Meas 41:S78–S99
35. Yoshimura EM, Yukihara EG (2006) Optically stimulated luminescence: searching for new dosimetric materials. Nucl Instrum Methods Phys Res, Sect B 250:337–341
36. Pisarska J (2009) Luminescence behavior of Dy^{3+} ions in lead borate glasses. Opt Mater 31:1784–1786
37. Pisarski WA, Dominiak-Dzik G, Ryba-Romanowski W, Pisarska J (2008) Role of PbO substitution by PbF_2 on structural behavior and luminescence of rare earth-doped lead borate glass. J Alloy Compd 451:220–222

38. Pisarska J, Pisarski WA, Ryba-Romanowski W (2010) Laser spectroscopy of Nd^{3+} and Dy^{3+} ions in lead borate glasses. Opt Laser Technol 42:805–809
39. Tanabe S, Kang J, Hanada T, Soga N (1998) Yellow/blue luminescences of Dy^{3+}-doped borate glasses and their anomalous temperature variations. J Non-Cryst Solids 239:170–175
40. Pisarska J, Lisiecki R, Ryba-Romanowski W, Goryczka T, Pisarski WA (2010) Unusual luminescence behavior of Dy^{3+}-doped lead borate glass after heat treatment. Chem Phys Lett 489:198–201
41. Tiefeng X, Feifei C, Shixun D, Qiuhua N, Xiang S, Xunsi W (2009) Third-order optical nonlinear characterizations of Bi_2O_3–B_2O_3–TiO_2 ternary glasses. Phys B 404:2012–2015
42. Chen Y, Huang Y, Huang M, Chen R, Luo Z (2005) Effect of Nd^{3+} on the spectroscopic properties of bismuth borate glasses. J Am Ceram Soc 88:19–23
43. Chen Y, Huang Y, Huang M, Chen R, Luo Z (2004) Spectroscopic properties of Er^{3+} ions in bismuth borate glasses. Opt Mater 25:271–278
44. Raju CN, Reddy CA, Sailaja S, Seo HJ, Reddy BS (2012) Judd-Ofelt theory: optical absorption and NIR emission spectral studies of Nd^{3+}: CdO–Bi_2O_3–B_2O_3 glasses for laser applications. J Mater Sci 47:772–778. doi:10.1007/s10853-011-5853-5
45. Pisarski WA, Pisarska J, Dominiak-Dzik G, Ryba-Romanowski W (2009) Transition metal (Cr^{3+}) and rare earth (Eu^{3+}, Dy^{3+}) ions used as a spectroscopic probe in compositional-dependent lead borate glasses. J Alloy Compd 484:45–49
46. Hench LL (1991) Bioceramics: from concept to clinic. J Am Ceram Soc 74:1487–1510
47. Rahaman MN, Day DE, Bal BS, Fu Q, Jung SB, Bonewald LF, Tomsia AP (2011) Bioactive glass in tissue engineering. Acta Biomater 7:2355–2373
48. Gu Y, Xiao W, Lu L, Huang W, Rahaman MN, Wang D (2011) Kinetics and mechanisms of converting bioactive borate glasses to hydroxyapatite in aqueous phosphate solution. J Mater Sci 46:47–54. doi:10.1007/s10853-010-4792-x
49. Hakki SS, Bozkurt BS, Hakki EE (2010) Boron regulates mineralized tissue-associated proteins in osteoblasts (MC3T3-E1). J Trace Elem Med Biol 24:243–250
50. Pan HB, Zhao XL, Zhang X, Zhang KB, Li LC, Li ZY, Lam WM, Lu WW, Wang DP, Huang WH, Lin KL, Chang J (2010) Strontium borate glass: potential biomaterial for bone regeneration. J Royal Soc Interface 7:1025–1031
51. Bi L, Rahaman MN, Day DE, Brown Z, Samujh C, Liu X, Mohammadkhah A, Dusevich V, Eick JD, Bonewald LF (2013) Effect of bioactive borate glass microstructure on bone regeneration, angiogenesis, and hydroxyapatite conversion in a rat calvarial defect model. Acta Biomater 9:8015–8026
52. Peddi L, Brow RK, Brown RF (2008) Bioactive borate glass coatings for titanium alloys. J Mater Sci Mater Med 19:3145–3152
53. Brow RK, Saha SK, Goldstein JI (1993) Interfacial reactions between titanium and borate glass. In: MRS Proceedings, vol 314. Cambridge University Press, p 77
54. Marion NW, Liang W, Liang W, Reilly GC, Day DE, Rahaman MN, Mao JJ (2005) Borate glass supports the in vitro osteogenic differentiation of human mesenchymal stem cells. Mech Adv Mater Struct 12:239–246
55. Carta D, Knowles JC, Guerry P, Smith ME, Newport RJ (2009) Sol–gel synthesis and structural characterisation of P_2O_5–B_2O_3–Na_2O glasses for biomedical applications. J Mater Chem 19:150–158
56. Bengisu M, Yilmaz E (2004) Chemical durability of alumina and selected glasses in simulated body fluid: effect of composition and surface abrasion. Adv Exp Med Biol 553:103–112
57. Brown RF, Teitelbaum HK, Adams N, Brow RK (2002) In vitro assessment of a novel borate-based bioactive glass, MRS Spring Meeting, San Fransisco. http://mse.mst.edu/research/crbet. Accessed 12 June 2015
58. Liu X, Xie Z, Zhang C, Pan H, Rahaman MN, Zhang X, Pan H, Rahaman MN, Zhang X, Fu Q, Huang W (2010) Bioactive borate glass scaffolds: in vitro and in vivo evaluation for use as a drug delivery system in the treatment of bone infection. J Mater Sci Mater Med 21:575–582
59. Xie Z, Liu X, Jia W, Zhang C, Huang W, Wang J (2009) Treatment of osteomyelitis and repair of bone defect by degradable bioactive borate glass releasing vancomycin. J Control Release 139:118–126
60. Hum J, Boccaccini AR (2012) Bioactive glasses as carriers for bioactive molecules and therapeutic drugs: a review. J Mater Sci Mater Med 23:2317–2333
61. Wray P (2013) Wound healing: an update on Mo-Sci's novel borate glass fibers. Am Ceram Soc Bull 92:30–35
62. Mo-Sci Corporation (2015) Bioactive glass. http://www.mo-sci.com/bioactive-glass/ Accessed 4 Sept 2015
63. Kessler S, Fechner JH, Seneschal K, Zimmer J (2008) Glass compositions as an antimicrobial additive for dental materials. U.S. Patent No. 20,080,153,068. U.S. Patent and Trademark Office, Washington, DC
64. Han X, Du M, Ma Y, Day DE (2008) Evaluation of hydroxyapatite microspheres made from a borate glass to separate protein mixtures. J Mater Sci 43:5618–5625. doi:10.1007/s10853-008-2756-1
65. Ezz-Eldin FM (2001) Leaching and mechanical properties of cabal glasses developed as matrices for immobilization high-level wastes. Nucl Instr Methods Phys Res B 183:285–300
66. Remizov MB, Bogdanov AF, Vdovkina II, Biryukova MA (2005) Synthesis and use of borates of polyatomic alcohols for the preparation of liquid high-level wastes for ınclusion into borophosphate glass. At Energ 99:716–722
67. Erdogan C, Bengisu M, Erenturk SA (2014) Chemical durability and structural analysis of PbO–B_2O_3 glasses and testing for simulated radioactive wastes. J Nucl Mater 445:154–164
68. Singh N, Singh KJ, Singh K, Singh H (2004) Comparative study of lead borate and bismuth lead borate glass systems as gamma radiation shielding materials. Nucl Instr Methods Phys Res B 225:305–309
69. ElBatal FH, Marzouk MA (2011) Gamma rays interaction with bismuth borate glasses doped by transition metal ions. J Mater Sci 46:5140–5152. doi:10.1007/s10853-011-5445-4
70. Kaur S, Singh KJ (2013) Comparative study of lead borate and lead silicate glass systems doped with aluminum oxide as gamma-ray shielding materials. Int J Innov Technol Explor Eng 2:172–175
71. Ruengsri S (2014) Radiation shielding properties comparison of Pb-based silicate, borate, and phosphate glass matrices. Sci Technol Nucl Install 2014:1–6
72. Nascimento ML, Souza LA, Ferreira EB, Zanotto ED (2005) Can glass stability parameters infer glass forming ability? J Non-Cryst Solids 351:3296–3308
73. Feltz A (1993) Amorphous inorganic materials and glasses. VCH, Weinheim
74. Tanaka H (2005) Relationship among glass-forming ability, fragility, and short-range bond ordering of liquids. J Non-Cryst Solids 351:678–690
75. Cabral AA, Fredericci C, Zanotto ED (1997) A test of the Hruby parameter to estimate glass-forming ability. J Non-Cryst Solids 219:182–186
76. Hudon P, Baker DR (2002) The nature of phase separation in binary oxide melts and glasses. I. Silicate systems. J Non-Cryst Solids 303:299–345

77. Hudon P, Baker DR (2002) The nature of phase separation in binary oxide melts and glasses. II. Selective solution mechanism. J Non-Cryst Solids 303:346–353
78. Hudon P, Baker DR (2002) The nature of phase separation in binary oxide melts and glasses. III. Borate and germanate systems. J Non-Cryst Solids 303:354–371
79. Bengisu M (2001) Engineering ceramics. Springer, Berlin
80. Shaw RR, Uhlmann DR (1971) Effect of phase separation on the properties of simple glasses II. Elastic properties. J Non-Cryst Solids 5:237–263
81. Rawson H (1967) Inorganic glass forming systems. Academic Press, London
82. Levin EM, McDaniel CL (1962) The system Bi_2O–B_2O_3. J Am Ceram Soc 45:355–360
83. Levin EM, McMurdie HF (1949) The system BaO–B_2O_3. J Res Natl Bur Stand (US) 42:131–137
84. Levin EM (1966) Phase equilibria in the system niobium pentoxide-boric acid. J Res Natl Bur Stand (US) 70A:11–16
85. Levin EM, Robbins CR, Waring JL (1961) Immiscibility and the system lanthanum oxide–boric oxide. J Am Ceram Soc 44:87–91
86. Golubkov VV, Stolyarova VL (2011) Kinetics of early stages of phase separation in glasses of the PbO–B_2O_3 system. Glass Phys Chem 37:252–257
87. Shaw RR, Breedis JF (1972) Secondary phase separation in lead borate glasses. J Am Ceram Soc 55:422–425
88. Zhu D, Ray CS, Luo F, Zhou W, Day DE (2008) Melting and phase-separation of lead borate glasses in low gravity drop shaft. Ceram Int 34:417–420
89. Craievich AF, Zanotto EE, James PF (1983) Kinetics of subliquidus phase separation in silicate and borate glasses. A review. Bull Mineral 106:169–184
90. Shaw RR, Uhlmann DR (1968) Subliquidus immiscibility in binary alkali borates. J Am Ceram Soc 51:377–382
91. Charles RJ, Wagstaff FE (1968) Metastable immiscibility in the B_2O_3–SiO_2 system. J Am Ceram Soc 51:16–20
92. Porai-Koshits EA, Golubkov VV, Titov AP (1978) On the fluctuation structure of vitreous boron oxide and two-component alkali borate glasses. In: Pye LD, Frechette VD, Kreidl NJ (eds) Borate glasses: structure, properties, and applications, vol 12., Materials Science ResearchPlenum, New York, pp 183–199
93. Shelby JE (1983) Thermal expansion of alkali borate glasses. J Am Ceram Soc 66:225–227
94. Vogel W (1985) Chemistry of glass. The American Ceramic Society, Westerville
95. Du WF, Kuraoka K, Akai T, Yazawa T (2000) Study of kinetics of the phase separation in sodium borate glasses. J Mater Sci 35:3913–3921. doi:10.1023/A:1004845817600
96. Inoue S, Makishima A, Inoue H, Soga K, Konishi T, Asano T, Ishii Y, Koyama M (1997) In situ observation of phase separation of a barium borate melt in a stable immiscibility region under microgravity. J Am Ceram Soc 80:2413–2417
97. Inoue S, Wada K, Nukui A, Yamane M, Shibata S, Yasumori A, Yano T, Makishima A, Inoue H, Uo M, Fujimori Y (1995) Estimation of phase separation rates of PbO–B_2O_3 melts. J Mater Res 10:1561–1564
98. Brow RK, Watkins RD (1992) Sealing glasses for titanium and titanium alloys. U.S. Patent No. 5,104,738. U.S. Patent and Trademark Office, Washington, DC
99. Bunker BC (1994) Molecular mechanisms for corrosion of silica and silicate glasses. J Non-Cryst Solids 179:300–308
100. Bengisu M, Brow RK, Yilmaz E, Moguš-Milanković A, Reis ST (2006) Aluminoborate and aluminoborosilicate glasses with high chemical durability and the effect of P_2O_5 additions on the properties. J Non-Cryst Solids 352:3668–3676
101. Takaishi T, Jin J, Uchino T, Yoko T (2000) Structural study of PbO–B_2O_3 glasses by X-ray diffraction and 11B MAS NMR techniques. J Am Ceram Soc 83:2543–2548
102. Erdogan C, Akyil Erenturk S, Bengisu M (2010) Vitrification process for the immobilization of radioactive waste. Poster presentation, X. National Congress of Nuclear Science and Technology, Muğla, Turkey
103. Priven AI (2000) Calculation of the viscosity of glass-forming melts: V. Binary borate systems. Glass Phys Chem 26:541–558
104. Shelby JE (2003) Diffusion and solubility of water in alkali borate melts. Phys Chem Glasses Eur J Glass Sci Tech Part B 44:106–112
105. Shelby JE (2008) A limited review of water diffusivity and solubility in glasses and melts. J Am Ceram Soc 91:703–708
106. Zhang T, Fahrenholtz WG, Reis ST, Brow RK (2008) Borate volatility from SOFC sealing glasses. J Am Ceram Soc 91:2564–2569
107. Gunther C, Hofer G, Kleinlein W (1997) The stability of the sealing glass AF 45 in H_2/H_2O and O_2/N_2 atmospheres. In: Proceedings 5th international symposium solid oxide fuel cells, vol 97, pp 746–756
108. Snyder MJ, Mesko MG, Shelby JE (2006) Volatilization of boron from E-glass melts. J Non-Cryst Solids 352:669–673
109. Khanna A (2000) Effects of melt annealing on the mechanical and optical properties of lead borate glasses. Phys Chem Glasses-Eur J Glass Sci Tech Part B 41:330–332
110. Khanna A, Sawhney KJS, Tiwari MK, Bhardwaj S, Awasthi AM (2003) Effects of melt ageing on the density, elastic modulus and glass transition temperature of bismuth borate glasses. J Phys 15:6659–6670
111. Anzai Y, Terashima K, Kimura S (1993) Physical properties of molten lithium tetraborate. J Crys Growth 134:235–239
112. Huang WC, Jain H, Kamitsos EI, Patsis AP (1993) Anomalous expansion of sodium triborate melt and its effect on glass properties. J Non-Cryst Solids 162:107–117
113. Puttlitz KJ, Stalter KA (2004) Handbook of lead-free solder technology for microelectronic assemblies. CRC Press, New York
114. Wong-Ng W, Roth RS, Vanderah T, McMurdie HF (2001) Phase equilibria and crystallography of ceramic oxides. J Res Natl Inst Stand Technol 106:1097–1134
115. Taylor WJ, Lessar JF, Halperin LE, Kraska RE (1998) Terminal comprised of a thin layer of titanium clad over niobium or platinum, platinum-iridium alloys or of pure titanium. US Patent No. 5,821,011. US Patent and Trademark Office, Washington, DC
116. Frysz CA, Harvey AHI, Prinzbach JM (2004) Mismatched compression glass-to-metal seal. US Patent No. 6,759,163. US Patent and Trademark Office, Washington, DC
117. Esashi M, Nakano A, Shoji S, Hebiguchi H (1990) Low-temperature silicon-to-silicon anodic bonding with intermediate low melting point glass. Sens Actuators A21-A23:931–934
118. Frieser RG (1975) Electrocomponent science and technology, vol 2. Gordon and Breach, New York
119. Taylor WJ, Lessar JF, Weiss DJ (1992) Battery with weldable feedthrough. US Patent No. 5,104,755. US Patent and Trademark Office, Washington, DC
120. Kodama M, Kojima S (2002) Anharmonicity and fragility in lithium borate glasses. J Thermal Anal Calorim 69:961–970
121. Lower NP, McRae JL, Feller HA, Betzen AR, Kapoor S, Affatigato M, Feller SA (2001) Physical properties of alkaline-earth and alkali borate glasses prepared over an extended range of compositions. J Non-Cryst Solids 293:669–675
122. Klyuev VP, Pevzner BZ (2002) The influence of aluminum oxide on the thermal expansion, glass transition temperature,

and viscosity of lithium and sodium aluminoborate glasses. Glass Phys Chem 28:207–220
123. Shelby JE (1974) Properties and structure of B_2O_3–GeO_2 glasses. J Appl Phys 45:5272–5277
124. Saddeek YB (2004) Structural analysis of alkali borate glasses. Phys B 344:163–175
125. Velez MH, Tuller HL, Uhlmann DR (1982) Chemical durability of lithium borate glasses. J Non-Cryst Solids 49:351–362
126. Inaba S, Fujino S, Morinaga K (1999) Young's modulus and compositional parameters of oxide glasses. J Am Ceram Soc 82:3501–3507
127. Gowda VV, Anavekar RV, Rao KJ (2005) Elastic properties of fast ion conducting lithium based borate glasses. J Non-Cryst Solids 351:3421–3429
128. Gao Y (2005) Dependence of the mixed alkali effect on temperature and total alkali oxide content in $y[xLi_2O.(1-x)Na_2O].(1-y)B_2O_3$ glasses. J Solid State Chem 178:3376–3380
129. Donald IW, Metcalfe BL, Bradley DJ, Hill MJC, McGrath JL, Bye AD (1994) The preparation and properties of some lithium borate based glasses. J Mater Sci 29:6379–6396. doi:10.1007/BF00353994
130. Doweidar H, El-Damrawi GM, Moustafa YM, Ramadan RM (2005) Density of mixed alkali borate glasses: a structural analysis. Phys B 362:123–132
131. Levin EM, Block S (1957) Structural interpretation of immiscibility in oxide systems: I, analysis and calculation of immiscibility. J Am Ceram Soc 40:95–106
132. Chryssikos GD, Liu L, Varsamis CP, Kamitsos EI (1998) Dielectric and structural investigation of alkali triborate glasses. J Non-Cryst Solids 235:761–765
133. Ratai E, Janssen M, Eckert H (1998) Spatial distributions and chemical environments of cations in single-and mixed alkali borate glasses: evidence from solid state NMR. Solid State Ionics 105:25–37
134. Yun YH, Bray PJ (1981) B11 nuclear magnetic resonance studies of $Li_2O{\cdot}B_2O_3$ glasses of high Li_2O content. J Non-Cryst Solids 44:227–237
135. Goktas AA, Neilson GF, Weinberg MC (1992) Crystallization of lithium borate glasses. J Mater Sci 27:24–28. doi:10.1007/BF02403639
136. Royle M, MacKenzie J, Taylor J, Sharma M, Feller S (1994) Densities, glass transition temperatures, and structural models resulting from extremely modified caesium and rubidium borate glasses. J Non-Cryst Solids 177:242–248
137. Janssen M, Eckert H (2000) 11 B 23 Na Rotational echo double resonance NMR: a new approach for studying the spatial cation distribution in sodium borate glasses. Solid State Ionics 136:1007–1014
138. Kodama M (1991) Ultrasonic velocity in sodium borate glasses. J Mater Sci 26:4048–4053. doi:10.1007/BF00553487
139. Ahoussou AP, Rogez J, Kone A (2006) Enthalpy of mixing in 0.8 $[xB_2O_3$–$(1-x)\ P_2O_5]$–0.2 Na_2O glasses at 298K. Thermochim Acta 441:96–100
140. Klyuev VP, Pevzner BZ (2003) Thermal expansion and glass transition temperature of calcium borate and calcium aluminoborate glasses. Glass Phys Chem 29:127–136
141. Bajaj A, Khanna A, Kulkarni NK, Aggarwal SK (2009) Effects of doping trivalent ions in bismuth borate glasses. J Am Ceram Soc 92:1036–1041
142. Wu J, Stebbins JF (2014) Cation field strength effects on boron coordination in binary borate glasses. J Am Ceram Soc 97:2794–2801
143. Angel PW, Cooper AR (1997) Effect of melting time and temperature on properties of a sodium borate glass. J Non-Cryst Solids 221:70–77
144. Pevzner BZ, Klyuev VP (2004) Manifestation of the mixed-cation effect in dilatometric properties of RO $(R_2O){\cdot}2B_2O_3$ borate glasses upon replacement of Na_2O by BaO, Na_2O by MgO, and BaO by MgO. Glass Phys Chem 30:506–514
145. Becker P (2003) Thermal and optical properties of glasses of the system Bi_2O_3–B_2O_3. Cryst Res Technol 38:74–82
146. Cormier L, Majérus O, Neuville DR, Calas G (2006) Temperature-induced structural modifications between alkali borate glasses and melts. J Am Ceram Soc 89:13–19
147. Manupriya, Thind KS, Sharma G, Rajendran V, Singh K, Gayathri Devi AV, Aravindan S (2006) Structural and acoustic investigations of calcium borate glasses. Phys Status Solidi A 203:2356–2364
148. Mutluer T, Timucin M (1975) Phase equilibria in the system MgO–B_2O_3. J Am Ceram Soc 58:196–197
149. Kapoor S, George HB, Betzen A, Affatigato M, Feller S (2000) Physical properties of barium borate glasses determined over a wide range of compositions. J Non-Cryst Solids 270:215–222
150. Koudelka L, Mosner P (2000) Borophosphate glasses of the ZnO–B_2O_3–P_2O_5 system. Mater Lett 42:194–199
151. Hayashi A, Nakai M, Tatsumisago M, Minami T, Himei Y, Miura Y, Katada M (2002) Structural investigation of SnO–B_2O_3 glasses by solid-state NMR and X-ray photoelectron spectroscopy. J Non-Cryst Solids 306:227–237
152. Cheng Y, Xiao H, Guo W, Guo W (2007) Structure and crystallization kinetics of PbO–B_2O_3 glasses. Ceram Int 33:1341–1347
153. Zahra AM, Zahra CY, Piriou B (1993) DSC and Raman studies of lead borate and lead silicate glasses. J Non-Cryst Solids 155:45–55
154. Metwalli E (2003) Copper redox behavior, structure and properties of copper lead borate glasses. J Non-Cryst Solids 317:221–230
155. Bergeron CG, Russell CK, Friedberg AL (1963) Thermal analysis of lead borate glasses during crystallization. J Am Ceram Soc 46:246
156. Saddeek YB, Gaafar MS (2009) Physical and structural properties of some bismuth borate glasses. Mater Chem Phys 115:280–286
157. Yawale SP, Pakade SV (1993) DC conductivity and hopping mechanism in Bi_2O_3-B_2O_3 glasses. J Mater Sci 28:5451–5455. doi:10.1007/BF00367814
158. Bajaj A, Khanna A, Chen B, Longstaffe JG, Zwanziger UW, Zwanziger JW, Gomez Y, González F (2009) Structural investigation of bismuth borate glasses and crystalline phases. J Non-Cryst Solids 355:45–53
159. El-Damrawi G, El-Egili K (2001) Characterization of novel CeO_2–B_2O_3 glasses, structure and properties. Phys B 299:180–186
160. Hill GC, Holman JS (1995) Chemistry in context. Nelson Thornes, Cheltenham
161. Dell WJ, Bray PJ, Xiao SZ (1983) ^{11}B NMR studies and structural modeling of Na_2O–B_2O_3–SiO_2 glasses of high soda content. J Non-Cryst Solids 58:1–16
162. Du LS, Stebbins JF (2005) Network connectivity in aluminoborosilicate glasses: a high-resolution ^{11}B, 27 Al and ^{17}O NMR study. J Non-Cryst Solids 351:3508–3520
163. Bray PJ, Feller SA, Jellison GE, Yun YH (1980) B 10 NMR studies of the structure of borate glasses. J Non-Cryst Solids 38:93–98
164. Bray PF (1978) NMR studies of borates. In: Bye L, Frechette V, Kreidle N (eds) Materials science research 12, Proceedings of the conference on boron in glass and glass-ceramics, Plenum, New York, pp 321–351
165. Hayashi A, Nakai M, Tatsumisago M, Minami T (2002) Structure and properties of glasses in the system Li_2O–SnO–B_2O_3. CR Chim 5:751–757

166. Tomozawa M (1999) A source of the immiscibility controversy of borate and borosilicate glass systems. J Am Ceram Soc 82:206–208
167. Mazurin OV, Porai-Koshits EA (eds) (1984) Phase separation in glass. North Holland, Amsterdam
168. Kasper J, Feller S, Sumcad G, Boyd DC (1984) New sodium borate glasses. J Am Ceram Soc 67:c71–c72
169. Sycheva GA, Grishchenko LV (2008) Specific features of the glass formation in the R_2O–B_2O_3, R_2O–SiO_2, and R_2O–B_2O_3–SiO_2 (R = Rb, Cs) systems. Glass Phys Chem 34:260–264
170. Strnad Z (1986) Glass ceramic materials. Elsevier, Amsterdam
171. Ohta Y, Morinaga K, Yanagase T (1982) Liquid–liquid immiscibility in several binary borate systems. J Ceram Soc Jpn 90:511
172. Kim SS, Sanders TH (2003) Thermodynamic assessment of the miscibility gaps and the metastable liquidi in the B_2O_3–RO systems (R = Mg, Ca, Sr, and Ba). J Am Ceram Soc 86:1947–1952
173. Crichton SN, Tomozawa M (1997) Prediction of phase separation in binary borate glasses. J Non-Cryst Solids 215:244–251
174. Levin EM (1970) Phase diagrams. In: Alper AM (ed) Liquid immiscibility in oxide systems, vol III. Academic Press, New York, pp 143–236
175. Clemens K, Yoshiyagawa M, Tomozawa M (1981) Liquid–liquid immiscibility in barium oxide-boron oxide. J Am Ceram Soc 64:C91
176. Meera BN, Ramakrishna J (1993) Raman spectral studies of borate glasses. J Non-Cryst Solids 159:1–21
177. Dimitriev Y, Kashchieva E (1975) Immiscibility in the TeO_2–B_2O_3 system. J Mater Sci 10:1419–1424. doi:10.1007/BF00540832
178. Liedberg DJ, Ruderer CG, Bergeron CG (1965) Evidence of metastable immiscibility in the system PbO–B_2O_3. J Am Ceram Soc 48:440
179. Podlesny J, Weinberg MC, Neilson GF, Chen A (1993) Experimental determination of the binodal temperature in the lead borate system. J Mater Sci 28:1663–1666. doi:10.1007/BF00363365
180. Rabinovich EM (1976) Lead in glasses. J Mater Sci 11:925–948. doi:10.1007/BF00542311
181. Koudelka L, Mošner P, Zeyer M, Jäger C (2005) Structure and properties of mixed sodium–lead borophosphate glasses. J Non-Cryst Solids 351:1039–1045
182. Reis STD, Pontuschka WM, Yang JB, Faria DLA (2003) Properties and structural features of iron doped BABAL glasses. Mater Res 6:389–394
183. Youssef NH, Belkhiria MS, Videau JJ, Amara MB (2000) Investigation of the physico-chemical properties of calcium borophosphate glasses. Effect of the substitution of sodium for calcium. Mater Lett 44:269–274
184. Day DE, Wu Z, Ray CS, Hrma P (1998) Chemically durable iron phosphate glass wasteforms. J Non-Cryst Solids 241:1–12
185. Abdel-Baki M, Abdel-Wahaba FA, Radia A, El-Diasty F (2007) Factors affecting optical dispersion in borate glass systems. J Phys Chem Solids 68:1457–1470
186. Ahoussou AP, Rogez J, Kone A (2007) Thermodynamical miscibility in 0.8 $[xB_2O_3$–$(1 - x)$ $P_2O_5]$–0.2 K_2O glasses. J Non-Cryst Solids 353:271–275